

Two-grid hp -version discontinuous Galerkin finite element methods for quasilinear elliptic PDEs on agglomerated coarse meshes

Scott Congreve*

Paul Houston†

Abstract

This article considers the extension of two-grid hp -version discontinuous Galerkin finite element methods for the numerical approximation of second-order quasilinear elliptic boundary value problems of monotone type to the case when agglomerated polygonal/polyhedral meshes are employed for the coarse mesh approximation. We recall that within the two-grid setting, while it is necessary to solve a nonlinear problem on the coarse approximation space, only a linear problem must be computed on the original fine finite element space. In this article, the coarse space will be constructed by agglomerating elements from the original fine mesh. Here, we extend the existing *a priori* and *a posteriori* error analysis for the two-grid hp -version discontinuous Galerkin finite element method from [20] for coarse meshes consisting of standard element shapes to include arbitrarily agglomerated coarse grids. Moreover, we develop an hp -adaptive two-grid algorithm to adaptively design the fine and coarse finite element spaces; we stress that this is undertaken in a fully automatic manner, and hence can be viewed as blackbox solver. Numerical experiments are presented for two- and three-dimensional problems to demonstrate the computational performance of the proposed hp -adaptive two-grid method.

Keywords: discontinuous Galerkin finite element methods, polytopic elements, hp -finite element methods, two-grid methods, quasilinear PDEs

Mathematics Subject Classification (2010): 35J62, 65N30, 65N50

1 Introduction

In recent years there has been a tremendous amount of interest in the mathematical development and application of discretisation methods for the numerical approximation of partial differential equations (PDEs) which employ general polygonal/polyhedral (collectively referred to as polytopic) meshes; see, for example, [2, 8, 10, 13, 14, 15, 22, 23, 24], and the references cited therein. The exploitation of such general meshes is highly advantageous for the efficient approximation of localized geometrical features present in the underlying geometry. Indeed, in many geophysical and engineering applications, the numerical study of fluid-structure interaction, crack and wave propagation phenomena, and flow in fractured porous media, for example, are typically characterized by a strong complexity of the physical domain, cf. [3]. Furthermore, the ability to utilise polytopic meshes offers a number of advantages also in the context of multilevel linear solvers, such as Schwarz-based domain decomposition preconditioners and multigrid solvers, see, for example, [4, 6, 5], and the references cited therein. In this context, embedded coarse meshes can very easily be constructed using mesh agglomeration techniques. Here, collections of elements present in the

*Charles University, Faculty of Mathematics and Physics, Department of Numerical Mathematics, Sokolovská 83, 18675 Prague, Czech Republic. congreve@karlin.mff.cuni.cz

†School of Mathematical Sciences, University of Nottingham, University Park, Nottingham, NG7 2RD, UK. Paul.Houston@nottingham.ac.uk

original fine mesh are ‘glued’ together to form coarse polytopic elements; a very simple approach to define these coarse elements is to employ graph partitioning software, such as METIS [28], for example.

In the present paper we consider the application of polytopic meshes to design black box two-grid methods for the numerical approximation of nonlinear PDE problems. Two-grid methods were originally introduced by [43, 44, 45] in the context of standard Galerkin finite element methods for both non-symmetric linear and nonlinear problems, cf., for example, [7, 11, 12, 21, 30, 39, 42], and the references cited therein. Extensions to discontinuous Galerkin methods (DGFEMs) have been undertaken in [12, 18, 20], for example. Indeed, in our own previous work [18, 20] we have studied both the *a priori* and *a posteriori* error analysis for the two-grid variant of the *hp*-version interior penalty DGFEM for the numerical solution of strongly monotone second order quasilinear elliptic partial differential equations on so called standard meshes; by this we mean meshes comprising of simplicial, quadrilateral, and hexahedral elements.

We recall that the construction of two-grid methods for nonlinear PDE problems relies on the definition of a coarse finite element space X and fine space Y , where the coarse space is, hopefully, considerably coarser compared to the fine space. The method first solves the (expensive) full nonlinear problem on the coarse space X before utilizing this solution to linearize the underlying PDE problem on the fine space Y . Obtaining a solution on the fine space then only requires solving a *linear* problem, which is computationally cheaper than solving the full nonlinear problem. Previous work on two-grid methods generally assume that coarse and fine meshes can be easily constructed based on employing standard shaped elements in such a manner that $X \subset Y$; i.e., that the coarse mesh is embedded within the fine one. In practice, it may be necessary to construct a coarse mesh from an unstructured fine mesh, in which case, this condition may be difficult to satisfy when standard elements are employed. To that end, we shall consider development of two-grid methods whereby the coarse mesh is constructed by agglomerating fine mesh elements. In this way, the agglomerated coarse elements will consist of general polytopic elements. In particular, in this article, we study the *hp*-version of the two-grid incomplete interior penalty DGFEM. Here we generalise the analysis presented in [20] to the current setting, whereby the coarse mesh may be constructed via agglomeration. Moreover, we develop a general purpose black box two-grid adaptive algorithm which automatically refines both the fine and coarse spaces to ensure that the discretisation error is controlled in a computationally efficient manner.

The outline of this article is as follows. In Sect. 2 we introduce the underlying model problem, together with its two-grid *hp*-version DGFEM approximation. Next, in Sect. 3 we derive an *a priori* error bound for the proposed numerical scheme. Sect. 4 is devoted to the development of *hp*-version adaptive algorithms for automatically refining both the coarse and fine meshes. In Sect. 5, we perform numerical experiments to demonstrate the performance of the proposed adaptive strategy. Finally, in Sect. 6 we summarise the work presented in this article and discuss potential extensions.

2 Model problem and two-grid *hp*-version DGFEM

In this section we introduce a model second-order quasilinear elliptic boundary value problem and discuss its numerical approximation based on employing the two-grid DGFEM on a fine mesh comprising of standard elements, but with a coarse mesh consisting of elements constructed by agglomerating fine elements.

2.1 Model problem

In this article we consider the numerical approximation of the following quasilinear elliptic boundary value problem: find $u \in H^1(\Omega)$ such that

$$\begin{aligned} -\nabla \cdot (\mu(\mathbf{x}, |\nabla u|) \nabla u) &= f(\mathbf{x}) && \text{in } \Omega, \\ u &= 0 && \text{on } \Gamma. \end{aligned} \tag{1}$$

where Ω is a bounded polygonal/polyhedral Lipschitz domain in $\Omega \subset \mathbb{R}^d$, $d = 2, 3$ with boundary $\Gamma := \partial\Omega$ and $f \in L^2(\Omega)$.

Assumption 2.1. We assume that the nonlinearity μ satisfies the following conditions:

(A1) $\mu \in C^0(\overline{\Omega} \times [0, \infty))$ and

(A2) there exists positive constants m_μ and M_μ such that the following monotonicity property is satisfied:

$$m_\mu(t-s) \leq \mu(\mathbf{x}, t)t - \mu(\mathbf{x}, s)s \leq M_\mu(t-s), \quad t \geq s \geq 0, \mathbf{x} \in \overline{\Omega}. \quad (2)$$

From [29, Lemma 2.1] we note that, as μ satisfies (2), there exists constants C_1 and C_2 , $C_1 \geq C_2 > 0$, such that for all vectors $\mathbf{v}, \mathbf{w} \in \mathbb{R}^d$ and all $\mathbf{x} \in \overline{\Omega}$,

$$|\mu(\mathbf{x}, |\mathbf{v}|)\mathbf{v} - \mu(\mathbf{x}, |\mathbf{w}|)\mathbf{w}| \leq C_1|\mathbf{v} - \mathbf{w}|, \quad (3)$$

$$C_2|\mathbf{v} - \mathbf{w}|^2 \leq (\mu(\mathbf{x}, |\mathbf{v}|)\mathbf{v} - \mu(\mathbf{x}, |\mathbf{w}|)\mathbf{w}) \cdot (\mathbf{v} - \mathbf{w}). \quad (4)$$

For ease of notation we shall suppress the dependence of μ on \mathbf{x} and write $\mu(t)$ instead of $\mu(\mathbf{x}, t)$.

2.2 Meshes, spaces, and trace operators

Following [17] we consider a *fine* mesh \mathcal{T}_h which partitions $\Omega \subset \mathbb{R}^d$, $d = 2, 3$, into disjoint open-element domains κ such that $\overline{\Omega} = \bigcup_{\kappa \in \mathcal{T}_h} \overline{\kappa}$. We assume shape-regularity of the mesh and that each element $\kappa \in \mathcal{T}_h$ is an affine image of a reference element $\hat{\kappa}$; i.e., for each $\kappa \in \mathcal{T}_h$ there exists an affine mapping $T_\kappa : \hat{\kappa} \rightarrow \kappa$ such that $\kappa = T_\kappa(\hat{\kappa})$, where $\hat{\kappa}$ is the open cube $(-1, 1)^3$ in \mathbb{R}^3 and either the open triangle $\{(x, y) : -1 < x < 1, -1 < y < -x\}$ or the open square $(-1, 1)^2$ in \mathbb{R}^2 . We denote by h_κ the element diameter of $\kappa \in \mathcal{T}_h$ and \mathbf{n}_κ signifies the unit outward normal vector to κ . We allow the meshes to be 1-irregular, i.e., each face of any one element $\kappa \in \mathcal{T}_h$ contains at most one hanging node and each edge of each face contains at most one hanging node. Under this assumption we can construct an auxiliary 1-irregular mesh by subdividing all quadrilateral and hexahedral elements $\kappa \in \mathcal{T}_h$ whose edges contain at least one hanging node into 2^d sub-elements. We assume that triangular elements are *regularly reducible*, cf. [34], to eliminate hanging nodes in triangular elements on the auxiliary mesh. We point out that these conditions are necessary to ensure that Theorem 4.1 holds, cf. [20]. Additionally, we note that these assumptions imply that the family $\{\mathcal{T}_h\}_{h>0}$ is of *bounded local variation*, i.e., there exists a constant $\rho_1 \geq 1$, independent of element sizes, such that $\rho_1^{-1} \leq h_\kappa/h_{\kappa'} \leq \rho_1$, for any pair of elements $\kappa, \kappa' \in \mathcal{T}_h$ which share a common face $F = \partial\kappa \cap \partial\kappa'$.

For a non-negative integer p , we denote by $\mathcal{P}_p(\hat{\kappa})$ the space of polynomials of total degree p on $\hat{\kappa}$. When $\hat{\kappa}$ is a hypercube, we also consider $\mathcal{Q}_p(\hat{\kappa})$, the set of all tensor-product polynomials on $\hat{\kappa}$ of degree p in each coordinate direction. To each $\kappa \in \mathcal{T}_h$ we assign a polynomial degree p_κ and construct the vector $\mathbf{p} = \{p_\kappa : \kappa \in \mathcal{T}_h\}$. We suppose that \mathbf{p} is also of bounded local variation, i.e., there exists a constant $\rho_2 \geq 1$, independent of the element sizes and \mathbf{p} , such that, for any pair of neighboring elements $\kappa, \kappa' \in \mathcal{T}_h$, $\rho_2^{-1} \leq p_\kappa/p_{\kappa'} \leq \rho_2$. With this notation, we introduce the *fine* finite element space

$$V_{hp}(\mathcal{T}_h, \mathbf{p}) = \{v \in L^2(\Omega) : v|_\kappa \circ T_\kappa \in \mathcal{R}_{p_\kappa}(\hat{\kappa}), \kappa \in \mathcal{T}_h\},$$

where \mathcal{R} is either \mathcal{P} or \mathcal{Q} .

Next, we introduce a *coarse* mesh partition \mathcal{T}_H , consisting of general polytopes K constructed by agglomerating elements $\kappa \in \mathcal{T}_h$ from the fine mesh, such that $\overline{\Omega} = \bigcup_{K \in \mathcal{T}_H} \overline{K}$; i.e., for all $K \in \mathcal{T}_H$, there exists a set $\mathcal{T}_h(K) \subseteq \mathcal{T}_h$ of fine mesh elements such that $\overline{K} = \bigcup_{\kappa \in \mathcal{T}_h(K)} \overline{\kappa}$, $\mathcal{T}_h = \bigcup_{K \in \mathcal{T}_H} \mathcal{T}_h(K)$, and, for all $\kappa \in \mathcal{T}_h$,

$$\kappa \in \mathcal{T}_h(K) \implies \kappa \notin \mathcal{T}_h(K') \quad \forall K' \in \mathcal{T}_H \setminus \{K\}.$$

We denote by H_κ the diameter of the coarse element $K \in \mathcal{T}_H$; i.e., $H_K = \text{diam}(K)$. To each $K \in \mathcal{T}_H$ we assign a polynomial degree P_K and construct the vector $\mathbf{P} = \{P_K : K \in \mathcal{T}_H\}$. We also assume that the polynomial degree of the coarse mesh element is less than or equal to the polynomial degree of its constituent fine mesh elements; i.e., $P_K \leq p_\kappa$ for all $K \in \mathcal{T}_H$ and $\kappa \in \mathcal{T}_h(K)$. We can then introduce the finite element space on the coarse mesh by

$$V_{HP}(\mathcal{T}_H, \mathbf{P}) = \{v \in L^2(\Omega) : v|_K \in \mathcal{P}_{P_K}(K), K \in \mathcal{T}_H\}.$$

We note that due to the assumptions on the polynomial degree that $V_{HP}(\mathcal{T}_H, \mathbf{P}) \subseteq V_{hp}(\mathcal{T}_h, \mathbf{p})$.

We shall now define some suitable face operators required for the definition of the proposed DGFEM. To this end we denote by \mathcal{F}_h^I the set of all interior faces of the fine mesh partition \mathcal{T}_h of Ω , and by \mathcal{F}_h^B the set of all boundary faces of the fine mesh \mathcal{T}_h . Additionally, we let $\mathcal{F}_h = \mathcal{F}_h^I \cup \mathcal{F}_h^B$ denote the set of all faces in the mesh \mathcal{T}_h . We similarly denote by \mathcal{F}_H^I , \mathcal{F}_H^B , and $\mathcal{F}_H = \mathcal{F}_H^I \cup \mathcal{F}_H^B$ the faces on the coarse mesh \mathcal{T}_H following [13]. Due to the construction of the coarse mesh via agglomeration of fine mesh elements we note that $\mathcal{F}_H \subset \mathcal{F}_h$, $\mathcal{F}_H^I \subset \mathcal{F}_h^I$, and $\mathcal{F}_H^B \subset \mathcal{F}_h^B$.

Let v and \mathbf{q} be scalar- and vector-valued functions, respectively, which are smooth inside each element $\kappa \in \mathcal{T}_h$. Given two adjacent elements, $\kappa^+, \kappa^- \in \mathcal{T}_h$ which share a common face $F \in \mathcal{F}_h^I$, i.e., $F = \partial\kappa^+ \cap \partial\kappa^-$, we write v^\pm and \mathbf{q}^\pm to denote the traces of the functions v and \mathbf{q} , respectively, on the faces F , taken from the interior of κ^\pm , respectively. Using this notation, we define the averages of v and \mathbf{q} at $\mathbf{x} \in F$ by

$$\{\{v\}\} = \frac{1}{2}(v^+ + v^-), \quad \{\{\mathbf{q}\}\} = \frac{1}{2}(\mathbf{q}^+ + \mathbf{q}^-),$$

respectively. Similarly, we define the jumps of v and \mathbf{q} at $\mathbf{x} \in F$ as

$$[[v]] = v^+ \mathbf{n}_{\kappa^+} + v^- \mathbf{n}_{\kappa^-}, \quad [[\mathbf{q}]] = \mathbf{q}^+ \cdot \mathbf{n}_{\kappa^+} + \mathbf{q}^- \cdot \mathbf{n}_{\kappa^-},$$

respectively. On a boundary face $F \in \mathcal{F}_h^B$, we set $\{\{v\}\} = v$, $\{\{\mathbf{q}\}\} = \mathbf{q}$, $[[v]] = v\mathbf{n}$, and $[[\mathbf{q}]] = \mathbf{q} \cdot \mathbf{n}$, where \mathbf{n} denotes the unit outward normal vector on Γ . We define $\{\{\cdot\}\}$ and $[[\cdot]]$ analogously on \mathcal{F}_H .

For a face $F \in \mathcal{F}_h$ of the fine mesh, we define h_F to be the diameter of the face and the face polynomial degree p_F to be defined by

$$p_F = \begin{cases} \max(p_\kappa, p_{\kappa'}), & \text{if } F = \partial\kappa \cap \partial\kappa' \in \mathcal{F}_h^I, \\ p_\kappa, & \text{if } F = \partial\kappa \cap \Gamma \in \mathcal{F}_h^B. \end{cases}$$

2.3 DGFEM discretization

With the notation introduced in the previous section we first define, for comparison with the proposed two-grid method (see below), the following *standard* DGFEM, based on employing an incomplete interior penalty formulation, on the fine space $V_{hp}(\mathcal{T}_h, \mathbf{p})$, for the numerical approximation of the problem (1): find $u_{hp} \in V_{hp}(\mathcal{T}_h, \mathbf{p})$ such that

$$A_{hp}(u_{hp}; u_{hp}, v_{hp}) = F_{hp}(v_{hp}) \quad (5)$$

for all $v_{hp} \in V_{hp}(\mathcal{T}_h, \mathbf{p})$, where

$$\begin{aligned} A_{hp}(\phi; u, v) &= \sum_{\kappa \in \mathcal{T}_h} \int_{\kappa} \mu(|\nabla\phi|) \nabla u \cdot \nabla v \, d\mathbf{x} - \sum_{F \in \mathcal{F}_h} \int_F \{\{\mu(|\nabla_h\phi|) \nabla_h u\}\} \cdot [[v]] \, ds \\ &\quad + \sum_{F \in \mathcal{F}_h} \int_F \sigma_{hp}[[u]] \cdot [[v]] \, ds, \\ F_{hp}(v) &= \sum_{\kappa \in \mathcal{T}_h} \int_{\kappa} f v \, d\mathbf{x}, \end{aligned}$$

and ∇_h is used to denote the broken gradient operator, defined element-wise. Here, the *fine grid interior penalty parameter* σ_{hp} is defined as

$$\sigma_{hp} = \gamma_{hp} \frac{p_F^2}{h_F}, \quad (6)$$

where $\gamma_{hp} > 0$ is a sufficiently large constant; cf. Lemma 2.2 below.

On the class of spaces $H^1(\Omega) + V_{hp}(\mathcal{T}_h, \mathbf{p})$, we introduce the following DGFEM *energy norm*

$$\|v\|_{hp}^2 = \|\nabla_h v\|_{L^2(\Omega)}^2 + \sum_{F \in \mathcal{F}_h} \int_F \sigma_{hp} |[v]|^2 ds. \quad (7)$$

Following [20], we recall that the form $A_{hp}(\phi; \cdot, \cdot)$, $\phi \in V_{hp}(\mathcal{T}_h, \mathbf{p})$, is coercive, in the sense that the following lemma holds.

Lemma 2.2. *There exists a positive constant γ_{\min} , such that for any $\gamma_{hp} > \gamma_{\min}$, there exists a coercivity constant $C_c > 0$, independent of h and \mathbf{p} , such that*

$$A_{hp}(\phi; v, v) \geq C_c \|v\|_{hp}^2$$

for all $\phi, v \in V_{hp}(\mathcal{T}_h, \mathbf{p})$.

Finally, we introduce the following hp -version of the two-grid DGFEM approximation to (1) based on employing the fine and coarse finite element spaces $V_{hp}(\mathcal{T}_h, \mathbf{p})$ and $V_{HP}(\mathcal{T}_H, \mathbf{P})$, respectively, cf. [12, Algorithm 1] and [20, Sect. 2.3]:

1. (Nonlinear solve) Compute the coarse grid approximation $u_{HP} \in V_{HP}(\mathcal{T}_H, \mathbf{P})$ such that

$$A_{HP}(u_{HP}; u_{HP}, v_{HP}) = F_{HP}(v_{HP}) \quad (8)$$

for all $v_{HP} \in V_{HP}(\mathcal{T}_H, \mathbf{P})$.

2. (Linear solve) Determine the fine grid solution $u_{2G} \in V_{hp}(\mathcal{T}_h, \mathbf{p})$ such that

$$A_{hp}(u_{HP}; u_{2G}, v_{hp}) = F_{hp}(v_{hp}) \quad (9)$$

for all $v_{hp} \in V_{hp}(\mathcal{T}_h, \mathbf{p})$.

Here, we note that $F_{HP}(\cdot)$ is defined analogously to $F_{hp}(\cdot)$ and $A_{HP}(\cdot; \cdot, \cdot)$ is defined on the coarse mesh partition \mathcal{T}_H analogously to $A_{hp}(\cdot; \cdot, \cdot)$, but with a different *coarse mesh interior penalty parameter* σ_{HP} ; the definition of σ_{HP} is given below in (10).

Remark 2.3. While the above DGFEM formulation is based on employing the incomplete interior penalty method, we stress that the proceeding error analysis naturally generalises to other DGFEMs commonly employed within the literature.

2.4 Inverse estimates and approximation results for the coarse space

Before embarking on the error analysis of the two-grid DGFEM defined in (8)–(9), we first derive some preliminary results. In particular, we revisit some inverse estimates and polynomial approximation results which are valid on general polytopic elements and are hence required to analyze the coarse grid approximation (8). To this end, we first introduce the necessary definitions and assumptions from [13, Section 3.2 & 4.3] required for the inverse inequality Lemma 2.6.

Definition 2.4. For each element $K \in \mathcal{T}_H$ we define the family \mathcal{F}_b^K of all possible d -dimensional simplices contained in K and having at least one face in common with K . Moreover, we write K_b^F to denote a simplex belonging to \mathcal{F}_b^K which shares with $K \in \mathcal{T}_H$ the specific face $F \subset \partial K$.

Assumption 2.5. For any $K \in \mathcal{T}_H$, there exists a set of non-overlapping d -dimensional simplices $\{K_b^F\} \subset \mathcal{F}_b^K$ contained within K , such that for all $F \subset \partial K$, the following condition holds

$$h_K \leq C_s \frac{d|K_b^F|}{|F|},$$

where C_s is a positive constant, which is independent of the discretization parameters, the number of faces that the element possesses, and the measure of F .

Equipped with these definitions we state the following inverse inequality from [13, Lemma 32].

Lemma 2.6. *Let $K \in \mathcal{T}_H$; then, for all $F \subset \partial K$, assuming Assumption 2.5 is satisfied, the inverse inequality*

$$\|v\|_{L^2(\partial K)}^2 \leq C_s C_{INV} d \frac{P^2}{H_K} \|v\|_{L^2(K)}^2$$

holds, for each $v \in \mathcal{P}_P(K)$, where C_s is the constant from Assumption 2.5 which is independent of $|K|/\sup_{K_b^F \subset K} |K_b^F|$, $|F|$, P , and v ; moreover, C_{INV} is a positive constant arising from a standard inverse inequality on simplices, and is independent of v , P , and H_K .

We now turn our attention to the derivation of suitable hp -version approximation results for the coarse finite element space. To this end, we define a covering for the coarse mesh as follows; cf. [13, Definition 17].

Definition 2.7. We define the covering $\mathcal{T}_H^\sharp = \{\mathcal{K}\}$ related to the coarse mesh \mathcal{T}_H as a set of open shape-regular d -simplices \mathcal{K} , such that, for each $K \in \mathcal{T}_H$, there exists a $\mathcal{K} \in \mathcal{T}_H^\sharp$, such that $K \subset \mathcal{K}$.

With this notation, we make the following assumption.

Assumption 2.8. We assume there exists a covering such that $h_{\mathcal{K}} := \text{diam}(\mathcal{K}) \leq C_D H_K$, for each pair $K \in \mathcal{T}_H$, $\mathcal{K} \in \mathcal{T}_H^\sharp$, with $K \subset \mathcal{K}$, for a constant $C_D > 0$, uniformly with respect to the mesh size.

Furthermore, we require the definition of the following classical extension operator, cf. [38].

Theorem 2.9. *Let D be a domain with minimally smooth boundary ∂D . Then, there exists a linear operator $\mathfrak{E} : H^s(D) \rightarrow H^s(\mathbb{R}^d)$, $s \in \mathbb{N}_0$, such that $\mathfrak{E}v|_D = v$ and*

$$\|\mathfrak{E}v\|_{H^s(\mathbb{R}^d)} \leq C_{\mathfrak{E}} \|v\|_{H^s(D)},$$

where $C_{\mathfrak{E}}$ is a positive constant depending only on s and parameters which characterize the boundary ∂D .

With this notation we state the following approximation result from [13, Lemmas 23 & 33].

Lemma 2.10. *Let $K \in \mathcal{T}_H$ and $\mathcal{K} \in \mathcal{T}_H^\sharp$ be the corresponding simplex, such that $K \subset \mathcal{K}$, cf. Definition 2.7. Suppose that $v \in L^2(\Omega)$ is such that $\mathfrak{E}v|_{\mathcal{K}} \in H^{L_K}(\mathcal{K})$, for some $L_K \geq 0$. Then, given Assumption 2.8 is satisfied, there exists $\Pi v \in V_{HP}(\mathcal{T}_H, \mathbf{P})$, such that $\Pi v|_K \in \mathcal{P}_{P_K}(K)$ and the following bound holds*

$$\|v - \Pi v\|_{H^q(K)} \leq C_{I,1} \frac{H_K^{S_K - q}}{P_K^{L_K - q}} \|\mathfrak{E}v\|_{H^{L_K}(\mathcal{K})}, \quad L_K \geq 0,$$

for $0 \leq q \leq L_K$. Furthermore, if $v \in H^1(\Omega)$ and Assumption 2.5 is satisfied then the following bound also holds

$$\|v - \Pi v\|_{L^2(\partial K)} \leq C_{I,2} \frac{H_K^{S_K - 1/2}}{P_K^{L_K - 1/2}} \|\mathfrak{E}v\|_{H^{L_K}(\mathcal{K})}, \quad L_K > 1/2.$$

Here, $S_K = \min(P_K + 1, L_K)$ and $C_{I,1}$ and $C_{I,2}$ are positive constants which depend on the shape-regularity of \mathcal{K} and the constant C_s from Assumption 2.5, but are independent of v , H_K , and P_K .

From the proof of Theorem 2.9 one can establish that the constant C_ϵ is independent of the measure of the underlying domain D , cf. [5]. Hence, employing Theorem 2.9, Lemma 2.10 may be stated in the following simplified form.

Corollary 2.11. *Under the assumptions of Lemma 2.10, the following bounds hold*

$$\begin{aligned} \|v - \Pi v\|_{H^q(K)} &\leq C'_{I,1} \frac{H_K^{S_K - q}}{P_K^{L_K - q}} \|v\|_{H^{L_K}(K)}, & L_K \geq 0, \quad 0 \leq q \leq L_K, \\ \|v - \Pi v\|_{L^2(\partial K)} &\leq C'_{I,2} \frac{H_K^{S_K - 1/2}}{P_K^{L_K - 1/2}} \|v\|_{H^{L_K}(K)}, & L_K > 1/2. \end{aligned}$$

Hence, the condition employed in [13, 14] regarding the amount of overlap of the simplices \mathcal{K} is not required.

2.5 Stability analysis of the coarse grid approximation

Based on the inverse inequality stated in Lemma 2.6, following [13, Lemma 35], we define the coarse mesh interior penalty parameter σ_{HP} as follows:

$$\sigma_{HP} = \begin{cases} \gamma_{HP} \max_{K \in \{K^+, K^-\}} \left(C_{\text{INV}} \frac{P_K^2}{H_K} \right), & \mathbf{x} \in F \in \mathcal{F}_H^I, F = \partial K^+ \cap \partial K^-, \\ \gamma_{HP} C_{\text{INV}} \frac{P_K^2}{H_K}, & \mathbf{x} \in F \in \mathcal{F}_H^B, F = \partial K^+ \cap \Gamma, \end{cases} \quad (10)$$

where $C_{\text{INV}}(P_K, K)$ is the constant from the inverse inequality Lemma 2.6 and $\gamma_{HP} > 0$ is a sufficiently large constant; cf. Lemma 2.12. We also define the DGFEM norm $\|\cdot\|_{HP}$ on the coarse mesh analogously to the fine mesh norm $\|\cdot\|_{hp}$ from (7) using the coarse mesh interior penalty parameter σ_{HP} defined above.

To analyze the hp -version DGFEM defined on the coarse mesh, cf. (8), in the case when general polytopic elements are employed, without introducing unnecessary regularity assumptions on the analytical solution u and only utilizing the hp -approximation results available on polytopic elements, the analysis presented in [20] must be generalized in a suitable manner. To this end, we introduce the following extension of the form $A_{HP}(\cdot; \cdot, \cdot)$, cf. [13, 35], to $\mathcal{V} \times \mathcal{V}$, where $\mathcal{V} = H^1(\Omega) + V_{HP}(\mathcal{T}_H, \mathbf{P})$:

$$\begin{aligned} \tilde{A}_{HP}(u, v) &= \sum_{K \in \mathcal{T}_H} \int_K \mu(|\nabla u|) \nabla u \cdot \nabla v \, d\mathbf{x} + \sum_{F \in \mathcal{F}_H} \int_F \sigma_{HP} [u] \cdot [v] \, ds \\ &\quad - \sum_{F \in \mathcal{F}_H} \int_F \{ \mu(|\mathbf{\Pi}_{L^2}(\nabla_h u)|) \mathbf{\Pi}_{L^2}(\nabla_h u) \} \cdot [v] \, ds. \end{aligned}$$

Here, $\mathbf{\Pi}_{L^2} : [L^2(\Omega)]^d \rightarrow [V_{HP}(\mathcal{T}_H, \mathbf{P})]^d$ denotes the orthogonal L^2 -projection onto the finite element space $[V_{HP}(\mathcal{T}_H, \mathbf{P})]^d$. We note, that

$$\tilde{A}_{HP}(u, v) = A_{HP}(u; u, v) \quad \text{for all } u, v \in V_{HP}(\mathcal{T}_H, \mathbf{P}).$$

The Lipschitz continuity and strong monotonicity for the extended form $\tilde{A}_{HP}(\cdot, \cdot)$ are determined in the following lemma.

Lemma 2.12. *Let $\gamma_{HP} \geq C_1^2 C_2^{-1} C_s d \epsilon$, where $\epsilon > 1/4$; then, given Assumption 2.5 holds, we have that the nonlinear form $\tilde{A}_{HP}(\cdot, \cdot)$ is strongly monotone in the sense that*

$$\tilde{A}_{HP}(v_1, v_1 - v_2) - \tilde{A}_{HP}(v_2, v_1 - v_2) \geq C_{\text{mono}} \|v_1 - v_2\|_{HP}^2 \quad \text{for all } v_1, v_2 \in \mathcal{V}, \quad (11)$$

and Lipschitz continuous in the sense that

$$|\tilde{A}_{HP}(v_1, w) - \tilde{A}_{HP}(v_2, w)| \leq C_{\text{cont}} \|v_1 - v_2\|_{HP} \|w\|_{HP} \quad \text{for all } v_1, v_2, w \in \mathcal{V}, \quad (12)$$

where C_{mono} and C_{cont} are positive constants independent of the discretization parameters.

Proof. The following proof proceeds in a similar manner to [13, Lemma 27] with modifications to account for the nonlinearity. Starting with the bound (11), we note by applying (4) that

$$\begin{aligned}
& \tilde{A}_{HP}(v_1, v_1 - v_2) - \tilde{A}_{HP}(v_2, v_1 - v_2) \\
& \geq C_2 \sum_{K \in \mathcal{T}_H} \|\nabla(v_1 - v_2)\|_{L^2(K)}^2 + \sum_{F \in \mathcal{F}_H} \|\sigma_{HP}^{1/2} \llbracket v_1 - v_2 \rrbracket\|_{L^2(F)}^2 \\
& \quad - \sum_{F \in \mathcal{F}_H} \int_F \left\{ \left\{ \mu(|\mathbf{\Pi}_{L^2}(\nabla_h v_1)|) \mathbf{\Pi}_{L^2}(\nabla_h v_1) \right. \right. \\
& \quad \quad \quad \left. \left. - \mu(|\mathbf{\Pi}_{L^2}(\nabla_h v_2)|) \mathbf{\Pi}_{L^2}(\nabla_h v_2) \right\} \cdot \llbracket v_1 - v_2 \rrbracket \right\} ds \\
& \equiv \text{I} + \text{II} + \text{III}. \tag{13}
\end{aligned}$$

We now proceed by considering Term III. To this end, for $F \in \mathcal{F}_H^T$, such that $F \subset \partial K^+ \cap \partial K^-$, upon application of (3), the Cauchy-Schwarz inequality, and the arithmetic-geometric mean inequality $ab \leq a^2\epsilon + b^2/(4\epsilon)$, $\epsilon > 0$, we deduce that

$$\begin{aligned}
& \int_F \left\{ \left\{ \mu(|\mathbf{\Pi}_{L^2}(\nabla_h v_1)|) \mathbf{\Pi}_{L^2}(\nabla_h v_1) \right. \right. \\
& \quad \left. \left. - \mu(|\mathbf{\Pi}_{L^2}(\nabla_h v_2)|) \mathbf{\Pi}_{L^2}(\nabla_h v_2) \right\} \cdot \llbracket v_1 - v_2 \rrbracket \right\} ds \\
& \leq C_1 \int_F \left\{ \left\{ \mathbf{\Pi}_{L^2}(\nabla_h(v_1 - v_2)) \right\} \right\} \llbracket v_1 - v_2 \rrbracket ds \\
& \leq C_1^2 \epsilon \left(\sum_{K \in \{K^+, K^-\}} \|\sigma_{HP}^{-1/2} \mathbf{\Pi}_{L^2}(\nabla_h(v_1 - v_2)|_K)\|_{L^2(F)}^2 \right) \\
& \quad + \frac{1}{8\epsilon} \|\sigma_{HP}^{1/2} \llbracket v_1 - v_2 \rrbracket\|_{L^2(F)}^2.
\end{aligned}$$

Analogously, for $F \in \mathcal{F}_H^B$, we have that

$$\begin{aligned}
& \int_F \left\{ \left\{ \mu(|\mathbf{\Pi}_{L^2}(\nabla_h v_1)|) \mathbf{\Pi}_{L^2}(\nabla_h v_1) \right. \right. \\
& \quad \left. \left. - \mu(|\mathbf{\Pi}_{L^2}(\nabla_h v_2)|) \mathbf{\Pi}_{L^2}(\nabla_h v_2) \right\} \cdot \llbracket v_1 - v_2 \rrbracket \right\} ds \\
& \leq C_1^2 \epsilon \|\sigma_{HP}^{-1/2} \mathbf{\Pi}_{L^2}(\nabla_h(v_1 - v_2))\|_{L^2(F)}^2 + \frac{1}{4\epsilon} \|\sigma_{HP}^{1/2} \llbracket v_1 - v_2 \rrbracket\|_{L^2(F)}^2.
\end{aligned}$$

Combining these results, employing the inverse inequality Lemma 2.6, the definition of σ_{HP} from (10), and the L^2 -stability of $\mathbf{\Pi}_{L^2}$, we have that

$$\begin{aligned}
\text{III} & \leq C_1^2 \epsilon \sum_{K \in \mathcal{T}_H} \sigma_{HP}^{-1} \|\mathbf{\Pi}_{L^2}(\nabla(v_1 - v_2))\|_{L^2(\partial K)}^2 + \frac{1}{4\epsilon} \sum_{F \in \mathcal{F}_H} \|\sigma_{HP}^{1/2} \llbracket v_1 - v_2 \rrbracket\|_{L^2(F)}^2 \\
& \leq \frac{C_1^2 \epsilon C_s d}{\gamma_{HP}} \sum_{K \in \mathcal{T}_H} \|\nabla(v_1 - v_2)\|_{L^2(K)}^2 + \frac{1}{4\epsilon} \sum_{F \in \mathcal{F}_H} \|\sigma_{HP}^{1/2} \llbracket v_1 - v_2 \rrbracket\|_{L^2(F)}^2.
\end{aligned}$$

Inserting this result into (13) gives

$$\begin{aligned}
\tilde{A}_{HP}(v_1, v_1 - v_2) - \tilde{A}_{HP}(v_2, v_1 - v_2) & \geq \left(C_2 - \frac{C_1^2 \epsilon C_s d}{\gamma_{HP}} \right) \sum_{K \in \mathcal{T}_H} \|\nabla(v_1 - v_2)\|_{L^2(K)}^2 \\
& \quad + \left(1 - \frac{1}{4\epsilon} \right) \sum_{F \in \mathcal{F}_H} \|\sigma_{HP}^{1/2} \llbracket v_1 - v_2 \rrbracket\|_{L^2(F)}^2.
\end{aligned}$$

Therefore, the nonlinear form $\tilde{A}_{HP}(\cdot, \cdot)$ is strongly monotone over $\mathcal{V} \times \mathcal{V}$, assuming that $\epsilon > 1/4$ and $\gamma_{HP} > C_1^2 C_2^{-1} C_s d \epsilon$.

We now consider the second bound (12). By applying (3) and Cauchy-Schwarz, we get that

$$\begin{aligned}
& |\tilde{A}_{HP}(v_1, w) - \tilde{A}_{HP}(v_2, w)| \\
& \leq C_1 \sum_{K \in \mathcal{T}_H} \|\nabla(v_1 - v_2)\|_{L^2(K)} \|\nabla w\|_{L^2(K)} \\
& \quad + \sum_{F \in \mathcal{F}_H} \|\sigma_{HP}^{1/2} [v_1 - v_2]\|_{L^2(F)} \|\sigma_{HP}^{1/2} [w]\|_{L^2(F)} \\
& \quad + \sum_{F \in \mathcal{F}_H} \int_F |\{\mu(|\mathbf{\Pi}_{L^2}(\nabla_h v_1)|) \mathbf{\Pi}_{L^2}(\nabla_h v_1) - \mu(|\mathbf{\Pi}_{L^2}(\nabla_h v_2)|) \mathbf{\Pi}_{L^2}(\nabla_h v_2)\}| \cdot [w]| \, ds.
\end{aligned}$$

Following a similar proof to the bound for (11), without the need to employ the arithmetic-geometric mean inequality, we deduce that

$$\begin{aligned}
& \sum_{F \in \mathcal{F}_H} \int_F |\{\mu(|\mathbf{\Pi}_{L^2}(\nabla_h v_1)|) \mathbf{\Pi}_{L^2}(\nabla_h v_1) - \mu(|\mathbf{\Pi}_{L^2}(\nabla_h v_2)|) \mathbf{\Pi}_{L^2}(\nabla_h v_2)\}| \cdot [w]| \, ds \\
& \leq C_1 \left(\frac{C_s d}{\gamma_{HP}} \sum_{K \in \mathcal{T}_H} \|\nabla(v_1 - v_2)\|_{L^2(K)}^2 \right)^{1/2} \left(\sum_{F \in \mathcal{F}_H} \|\sigma_{HP}^{1/2} [w]\|_{L^2(F)}^2 \right)^{1/2}.
\end{aligned}$$

A simple application of Cauchy-Schwarz completes the proof of Lipschitz continuity. \square

Theorem 2.13. *Suppose that γ_{hp} and γ_{HP} are sufficiently large; cf. Lemma 2.2 and Lemma 2.12, respectively. Then, there exists a unique solution $u_{2G} \in V_{hp}(\mathcal{T}_h, \mathbf{p})$ to the two-grid DGFEM (8)–(9).*

Proof. Given that Lemma 2.12 demonstrates Lipschitz continuity and strong monotonicity of the semi-linear form $\tilde{A}_{HP}(\cdot, \cdot)$, and

$$\tilde{A}_{HP}(u_{HP}, v_{HP}) = A_{HP}(u_{HP}; u_{HP}, v_{HP}) = F_{HP}(v_{HP})$$

for all $v_{HP} \in V_{HP}(\mathcal{T}_H, \mathbf{P})$, we can follow the proof of [25, Theorem 2.5] to show that u_{HP} is a unique solution of (8). Furthermore, as the fine grid formulation (9) is an interior penalty discretization of a linear elliptic PDE, where the coefficient $\mu(|\nabla_h u_{HP}|)$ is a known function, the existence and uniqueness of the solution u_{2G} to this problem follows immediately; cf., for example, [37, 41]. \square

3 Error analysis

In this section, we derive an *a priori* error bound for the two-grid DGFEM (8)–(9). To this end, we first establish an *a priori* error bound for the coarse mesh approximation defined by (8).

3.1 Coarse mesh *a priori* error bound

We first state and prove the following abstract error bound, derived in a similar manner to [13, Lemma 4.8].

Lemma 3.1. *Let $u \in H^1(\Omega)$ be the weak solution to (1) and $u_{HP} \in V_{HP}(\mathcal{T}_H, \mathbf{P})$ be the coarse mesh approximation defined by (8). Assuming that γ_{HP} is sufficiently large, cf. Lemma 2.12, the following abstract error bound holds.*

$$\begin{aligned}
\|u - u_{HP}\|_{HP} & \leq \left(1 + \frac{C_{\text{cont}}}{C_{\text{mono}}} \right) \inf_{v_{HP} \in V_{HP}(\mathcal{T}_H, \mathbf{P})} \|u - v_{HP}\|_{HP} \\
& \quad + \frac{1}{C_{\text{mono}}} \sup_{w_{HP} \in V_{HP}(\mathcal{T}_H, \mathbf{P}) \setminus \{0\}} \frac{|\tilde{A}_{HP}(u, w_{HP}) - F_{HP}(w_{HP})|}{\|w_{HP}\|_{HP}}.
\end{aligned}$$

Proof. The proof follows almost identically to [13, Lemma 28], using the strong monotonicity (11) and Lipschitz continuity (12) from Lemma 2.12. \square

We now state the following *hp*-version *a priori* error bound for the coarse mesh approximation defined by (8).

Theorem 3.2. *Let \mathcal{T}_H be a coarse mesh, constructed by agglomerating elements from a shape-regular fine mesh \mathcal{T}_h , satisfying Assumptions 2.5 and 2.8, with $\mathcal{T}_H^\sharp = \{\mathcal{K}\}$ an associated covering of \mathcal{T}_H consisting of d -simplices; cf. Definition 2.7. Let $u_{HP} \in V_{HP}(\mathcal{T}_H, \mathbf{P})$ be the coarse mesh approximation defined by (8). If the analytical solution $u \in H^1(\Omega)$ to (1) satisfies $u|_K \in H^{L_K}(K)$, $L_K \geq 3/2$, for $K \in \mathcal{T}_H$, such that $\mathfrak{E}u|_{\mathcal{K}} \in H^{L_K}(\mathcal{K})$, where $\mathcal{K} \in \mathcal{T}_H^\sharp$ with $K \subset \mathcal{K}$; then,*

$$\|u - u_{HP}\|_{HP}^2 \leq C_3 \sum_{K \in \mathcal{T}_H} \frac{H_K^{2S_K-2}}{P_K^{2L_K-2}} (1 + \mathcal{G}_K(H_K, P_K)) \|u\|_{H^{L_K}(K)}^2,$$

where $S_K = \min(P_K + 1, L_K)$,

$$\mathcal{G}_K(H_K, P_K) := \frac{P_K + P_K^2}{H_K} \max_{F \subset \partial K} \sigma_{HP}^{-1}|_F + \frac{H_K}{P_K} \max_{F \subset \partial K} \sigma_{HP}|_F$$

and C_3 is a positive constant, independent on the discretization parameters, but dependent on the constants m_μ , M_μ , C_1 , and C_2 from the monotonicity properties of $\mu(\cdot)$.

Proof. Following the proof in [13], upon application of Corollary 2.11 we get

$$\begin{aligned} & \inf_{v_{HP} \in V_{HP}(\mathcal{T}_H, \mathbf{P})} \|u - v_{HP}\|_{HP} \\ & \leq \|u - \Pi u\|_{HP}^2 \\ & \leq \sum_{K \in \mathcal{T}_H} \left(\|\nabla(u - \Pi u)\|_{L^2(K)}^2 + 2\sigma_{HP} \|(u - \Pi u)|_K\|_{L^2(\partial K)}^2 \right) \\ & \leq C \sum_{K \in \mathcal{T}_H} \frac{H_K^{2S_K-2}}{P_K^{2L_K-2}} \left(1 + \frac{H_K}{P_K} \max_{F \subset \partial K} \sigma_{HP}|_F \right) \|u\|_{H^{L_K}(K)}^2. \end{aligned} \quad (14)$$

Employing integration by parts, recalling the fact that u is the analytical solution to (1), $\mu \in C^0(\bar{\Omega} \times [0, \infty))$, and the bound (3), we deduce that

$$\begin{aligned} & |\tilde{A}_{HP}(u, w_{HP}) - F_{HP}(w_{HP})| \\ & = \left| \sum_{K \in \mathcal{T}_H} \int_{\partial K} \mu(|\nabla u|) \nabla u \cdot \mathbf{n}_K w_{HP} \, ds \right. \\ & \quad \left. - \sum_{F \in \mathcal{F}_H} \int_F \left\{ \mu(|\mathbf{\Pi}_{L^2}(\nabla_h u)|) \mathbf{\Pi}_{L^2}(\nabla_h u) \right\} \cdot [w_{HP}] \, ds \right| \\ & = \left| \sum_{F \in \mathcal{F}_H} \int_F \left\{ \mu(|\nabla_h u|) \nabla_h u - \mu(|\mathbf{\Pi}_{L^2}(\nabla_h u)|) \mathbf{\Pi}_{L^2}(\nabla_h u) \right\} \cdot [w_{HP}] \, ds \right| \\ & \leq C_1 \left(\sum_{F \in \mathcal{F}_H} \int_F \sigma_{HP}^{-1} \left\{ |\nabla_h u - \mathbf{\Pi}_{L^2}(\nabla_h u)| \right\} \, ds \right)^{1/2} \|w_{HP}\|_{HP}. \end{aligned}$$

By adding and subtracting $\mathbf{\Pi}(\nabla_h u)$ gives

$$\begin{aligned} & \sum_{F \in \mathcal{F}_H} \int_F \sigma_{HP}^{-1} \left\{ |\nabla_h u - \mathbf{\Pi}_{L^2}(\nabla_h u)| \right\}^2 \, ds \\ & \leq 2 \sum_{K \in \mathcal{T}_H} \left(\max_{F \subset \partial K} \sigma_{HP}^{-1}|_F \right) \left(\|\nabla u - \mathbf{\Pi}(\nabla u)\|_{L^2(\partial K)}^2 + \|\mathbf{\Pi}_{L^2}(\mathbf{\Pi}(\nabla u) - \nabla u)\|_{L^2(\partial K)}^2 \right). \end{aligned}$$

Applying the inverse inequality from Lemma 2.6 to the second term, followed by the approximation bounds stated in Corollary 2.11, together with the L^2 -stability of $\mathbf{\Pi}_{L^2}$, we get

$$\begin{aligned} & \sum_{F \in \mathcal{F}_H} \int_F \sigma_{HP}^{-1} \{ \|\nabla_h u - \mathbf{\Pi}_{L^2}(\nabla_h u)\| \}^2 ds \\ & \leq 2 \sum_{K \in \mathcal{T}_H} \left(\max_{F \subset \partial K} \sigma_{HP}^{-1} |F| \right) \left(C'_{I,2} \frac{H_K^{2S_K-3}}{P_K^{2L_K-3}} + C'_{I,1} C_s C_{\text{INV}} d \frac{H_K^{2S_K-3}}{P_K^{2L_K-4}} \right) \|u\|_{H^{L_K}(K)}^2. \end{aligned}$$

Combining (14) and the above bounds with Lemma 3.1 completes the proof. \square

3.2 Two-grid *a priori* error bound

We now consider the derivation of an *a priori* error bound for the two-grid DGFEM (8)–(9). To this end, we first recall the following *a priori* error bound for the standard DGFEM approximation (5) of the quasilinear problem (1).

Lemma 3.3. *Assuming that $u \in C^1(\Omega)$ and $u|_\kappa \in H^{l_\kappa}(\kappa)$, $l_\kappa \geq 2$, for $\kappa \in \mathcal{T}_h$ then the solution $u_{hp} \in V_{hp}(\mathcal{T}_h, \mathbf{p})$ of (5) satisfies the error bound*

$$\|u - u_{hp}\|_{hp}^2 \leq C_4 \sum_{\kappa \in \mathcal{T}_h} \frac{h_\kappa^{2s_\kappa-2}}{p_\kappa^{2l_\kappa-3}} \|u\|_{H^{l_\kappa}(\kappa)}^2,$$

with $1 \leq s_\kappa \leq \min(p_\kappa + 1, l_\kappa)$, $p_\kappa \geq 1$, for $\kappa \in \mathcal{T}_h$, and C_4 is a positive constant independent of u , h , and \mathbf{p} , but depends on the constants m_μ , M_μ , C_1 , and C_2 from the monotonicity properties of $\mu(\cdot)$.

Proof. See [25]. \square

Employing Theorem 3.2 and Lemma 3.3, we now deduce the following error bound for the two-grid approximation defined in (8)–(9).

Theorem 3.4. *Let \mathcal{T}_H be a coarse mesh, constructed by agglomerating elements from a shape-regular fine mesh \mathcal{T}_h , satisfying Assumptions 2.5 and 2.8, with $\mathcal{T}_H^\sharp = \{\mathcal{K}\}$ an associated covering of \mathcal{T}_H consisting of d -simplices; cf. Definition 2.7. If the analytical solution $u \in H^1(\Omega)$ to (1) satisfies $u|_\kappa \in H^{l_\kappa}(\kappa)$, $l_\kappa \geq 2$ and $u|_K \in H^{L_K}(K)$, $L_K \geq 3/2$, for $K \in \mathcal{T}_H$, such that $\mathfrak{E}u|_{\mathcal{K}} \in H^{L_K}(\mathcal{K})$, where $\mathcal{K} \in \mathcal{T}_H^\sharp$ with $K \subset \mathcal{K}$; then, the solution $u_{2G} \in V_{hp}(\mathcal{T}_h, \mathbf{p})$ of (9) satisfies the error bounds*

$$\begin{aligned} \|u_{hp} - u_{2G}\|_{hp}^2 & \leq C_4 C_5 \sum_{\kappa \in \mathcal{T}_h} \frac{h_\kappa^{2s_\kappa-2}}{p_\kappa^{2l_\kappa-3}} \|u\|_{H^{l_\kappa}(\kappa)}^2 \\ & \quad + C_3 C_5 \sum_{K \in \mathcal{T}_H} \frac{H_K^{2S_K-2}}{P_K^{2L_K-2}} (1 + \mathcal{G}_K(H_K, P_K)) \|u\|_{H^{L_K}(K)}^2, \\ \|u - u_{2G}\|_{hp}^2 & \leq (1 + C_5) C_4 \sum_{\kappa \in \mathcal{T}_h} \frac{h_\kappa^{2s_\kappa-2}}{p_\kappa^{2l_\kappa-3}} \|u\|_{H^{l_\kappa}(\kappa)}^2 \\ & \quad + C_3 C_5 \sum_{K \in \mathcal{T}_H} \frac{H_K^{2S_K-2}}{P_K^{2L_K-2}} (1 + \mathcal{G}_K(H_K, P_K)) \|u\|_{H^{L_K}(K)}^2, \end{aligned}$$

where $S_K = \min(P_K + 1, L_K)$, for $K \in \mathcal{T}_H$, $s_\kappa = \min(p_\kappa + 1, l_\kappa)$, for $\kappa \in \mathcal{T}_h$,

$$\mathcal{G}_K(H_K, P_K) := \frac{P_K + P_K^2}{H_K} \max_{F \subset \partial K} \sigma_{HP}^{-1} |F| + \frac{H_K}{P_K} \max_{F \subset \partial K} \sigma_{HP} |F|$$

and C_5 is a positive constant independent of u , h , H , \mathbf{p} , and \mathbf{P} , but depends on the constants m_μ , M_μ , C_1 , and C_2 from the monotonicity properties of $\mu(\cdot)$.

Remark 3.5. Assuming that \mathbf{P} is of local bounded variation, we note that due to the definition of σ_{HP} , and the fact that $P_K \geq 1$ for all $K \in \mathcal{T}_H$, we have that $\mathcal{G}_K(H_K, P_K) \leq CP_K$, for some positive constant C , independent of mesh size and polynomial degree. Therefore, we note that the terms in the second error bound have the same order for the polynomial degree and mesh size in both the coarse and fine mesh discretization parameters, which is analogous to the case when non-agglomerated coarse meshes, i.e. coarse meshes consisting of standard element types, are employed; cf. [20]

Proof. By application of the triangle inequality, we get

$$\|u - u_{2G}\|_{hp} \leq \|u - u_{hp}\|_{hp} + \|u_{2G} - u_{hp}\|_{hp};$$

hence, once the first bound stated in Theorem 3.4 has been established, then together with Lemma 3.3, the second bound follows immediately.

For the first bound, we follow the proof in [20, Theorem 3.1]. From the definition of the standard DGFEM formulation (5) and the fine grid approximation (9) we have that

$$A_{hp}(u_{hp}; u_{hp}, v_{hp}) = A_{hp}(u_{HP}; u_{2G}, v_{hp}) \quad \text{for all } v_{hp} \in V_{hp}(\mathcal{T}_h, \mathbf{p}).$$

Therefore, letting $\phi = u_{2G} - u_{hp} \in V_{hp}(\mathcal{T}_h, \mathbf{p})$, from Lemma 2.2, we deduce that

$$\begin{aligned} C_c \|\phi\|_{hp}^2 &\leq A_{hp}(u_{hp}; u_{hp}, \phi) - A_{hp}(u_{HP}; u_{hp}, \phi) \\ &\leq \sum_{\kappa \in \mathcal{T}_h} \int_{\kappa} |(\mu(|\nabla u_{hp}|) - \mu(|\nabla u_{HP}|)) \nabla u_{hp}| |\nabla \phi| \, d\mathbf{x} \\ &\quad + \sum_{F \in \mathcal{F}_h} \int_F \{ |(\mu(|\nabla_h u_{hp}|) - \mu(|\nabla_h u_{HP}|)) \nabla_h u_{hp}| \} \|\phi\| \, ds. \end{aligned}$$

Adding and subtracting $\mu(|\nabla u_{HP}|) \nabla u_{HP}$ to both terms on the right-hand side, then applying the triangle inequality, together with (2) and (3) gives

$$\begin{aligned} &\|\phi\|_{hp}^2 \\ &\leq \frac{C_1 + M_\mu}{C_c} \left(\sum_{\kappa \in \mathcal{T}_h} \int_{\kappa} |\nabla(u_{hp} - u_{HP})| |\nabla \phi| \, d\mathbf{x} + \sum_{F \in \mathcal{F}_h} \int_F \{ |\nabla_h(u_{hp} - u_{HP})| \} \|\phi\| \, ds \right) \\ &\leq \frac{C_1 + M_\mu}{C_c} \left(\left(\sum_{\kappa \in \mathcal{T}_h} \|\nabla(u - u_{hp})\|_{L^2(\kappa)}^2 + \sum_{F \in \mathcal{F}_h} \int_F \sigma_{hp}^{-1} \{ |\nabla_h(u - u_{hp})| \}^2 \, ds \right)^{1/2} \right. \\ &\quad \left. + \left(\sum_{K \in \mathcal{T}_H} \|\nabla(u - u_{HP})\|_{L^2(K)}^2 + \sum_{F \in \mathcal{F}_h} \int_F \sigma_{hp}^{-1} \{ |\nabla_h(u - u_{HP})| \}^2 \, ds \right)^{1/2} \right) \|\phi\|_{hp}. \end{aligned}$$

Therefore, applying a standard hp -version trace inequality, along with local bounded variation of the mesh parameters, we deduce that

$$\begin{aligned} &\|u_{2G} - u_{hp}\|_{hp} \\ &\leq \frac{\sqrt{C_5}}{2} \left(\left(\sum_{\kappa \in \mathcal{T}_h} \|\nabla(u - u_{hp})\|_{L^2(\kappa)}^2 \right)^{1/2} + \left(\sum_{K \in \mathcal{T}_H} \|\nabla(u - u_{HP})\|_{L^2(K)}^2 \right)^{1/2} \right), \end{aligned}$$

where C_5 is a positive constant independent of u , h , H , \mathbf{p} , and \mathbf{P} , but depends on the constants m_μ , M_μ , C_1 , and C_2 . Applying Lemma 3.3 and Theorem 3.2 completes the proof. \square

A numerical example validating these bounds can be found in our conference article [19].

4 *A posteriori* error estimation and two-grid *hp*-adaptive refinement

We note that the existing *a posteriori* error bound [20, Theorem 3.2] still holds for an agglomerated coarse mesh, as the only requirement on the coarse mesh is the fact that $V_{HP}(\mathcal{T}_H, \mathbf{P}) \subset V_{hp}(\mathcal{T}_h, \mathbf{p})$, which is still true in the current setting. For completeness we reproduce the error bound here.

Theorem 4.1. *Let $u \in H^1(\Omega)$ be the analytical solution of (1), $u_{HP} \in V_{HP}(\mathcal{T}_H, \mathbf{P})$ the numerical approximation obtained from (8), and $u_{2G} \in V_{hp}(\mathcal{T}_h, \mathbf{p})$ the numerical approximation computed from (9); then, the following *hp*-a posteriori error bound holds*

$$\|u - u_{2G}\|_{hp} \leq C_6 \left(\sum_{\kappa \in \mathcal{T}_h} (\eta_\kappa^2 + \xi_\kappa^2) + \sum_{\kappa \in \mathcal{T}_h} \|f - \Pi_{L^2} f\|_{L^2(\kappa)}^2 \right)^{1/2},$$

with a constant $C_6 > 0$, which is independent of \mathbf{h} , \mathbf{H} , \mathbf{p} , and \mathbf{P} . Here, Π_{L^2} is the L^2 -projection onto the fine grid finite element space $V_{hp}(\mathcal{T}_h, \mathbf{p})$, the local fine grid error indicators η_κ are defined, for all $\kappa \in \mathcal{T}_h$, by

$$\begin{aligned} \eta_\kappa^2 = & h_\kappa^2 p_\kappa^{-2} \|\Pi_{L^2} f + \nabla \cdot (\mu(|\nabla u_{HP}|) \nabla u_{2G})\|_{L^2(\kappa)}^2 \\ & + h_\kappa p_\kappa^{-1} \|\mu(|\nabla u_{HP}|) \nabla u_{2G}\|_{L^2(\partial\kappa \setminus \Gamma)}^2 + \gamma^2 h_\kappa^{-1} p_\kappa^3 \|u_{2G}\|_{L^2(\partial\kappa)}^2, \end{aligned} \quad (15)$$

and the local two-grid error indicators ξ_κ are defined, for all $\kappa \in \mathcal{T}_h$, by

$$\xi_\kappa^2 = \|(\mu(|\nabla u_{HP}|) - \mu(|\nabla u_{2G}|)) \nabla u_{2G}\|_{L^2(\kappa)}^2. \quad (16)$$

For the two-grid DGFEM discretization defined by (8)–(9) it is necessary to refine both fine and coarse meshes, together with their corresponding polynomial degree vectors, in order to decrease the error between u and u_{2G} with respect to the energy norm $\|\cdot\|_{hp}$. We note that, from Theorem 4.1, we have, for each fine element $\kappa \in \mathcal{T}_h$, a local error indicator η_κ and a local two-grid error indicator ξ_κ . The local error indicator η_κ is similar to the one which arises within the analysis of the standard DGFEM discretization and, hence, represents the error arising from the linear fine grid solve (9); whereas, the local two-grid error indicator ξ_κ represents the error stemming from the approximation of the nonlinear coefficient $\mu(|\nabla u_{hp}|)$ on the fine mesh by the nonlinear coefficient evaluated with respect to the coarse grid solution u_{HP} . To this end, we can consider a modified version of the two-grid mesh refinement algorithm [18, Algorithm 1 & Algorithm 2] to allow for a coarse mesh consisting of agglomerated fine mesh elements.

Algorithm 4.2. The fine and coarse finite element spaces $V_{hp}(\mathcal{T}_h, \mathbf{p})$ and $V_{HP}(\mathcal{T}_H, \mathbf{P})$ are refined as follows.

1. Initial Step: Select an initial fine mesh \mathcal{T}_h and initial fine mesh polynomial degree distribution \mathbf{p} . Create a coarse mesh \mathcal{T}_H by element agglomeration/graph partitioning (e.g., by METIS [28]) and assign a polynomial degree distribution \mathbf{P} , such that $V_{HP}(\mathcal{T}_H, \mathbf{P}) \subseteq V_{hp}(\mathcal{T}_h, \mathbf{p})$.
2. Solve (8)–(9) to determine u_{HP} and u_{2G} , respectively.
3. Select elements for refinement based on the local fine grid error indicators η_κ and the local two-grid error indicators ξ_κ , from (15) and (16), respectively:
 - (a) Determine the set $\mathfrak{R}(\mathcal{T}_h) \subseteq \mathcal{T}_h$ of *potential* elements to refine based on $\sqrt{\eta_\kappa^2 + \xi_\kappa^2}$ using a standard refinement strategy, e.g., the fixed fraction strategy.
 - (b) For all elements selected for refinement decided whether to perform refinement on the fine or coarse mesh. For all $\kappa \in \mathfrak{R}(\mathcal{T}_h)$:
 - if $\lambda_F \xi_\kappa \leq \eta_\kappa$ refine the fine element κ , and
 - if $\lambda_C \eta_\kappa \leq \xi_\kappa$ refine the coarse element $K \in \mathcal{T}_H$, where $\kappa \in \mathcal{T}_h(K)$.

4. Perform hp -refinement on the fine mesh \mathcal{T}_h using a standard refinement method; see, for example, [26, 31, 32, 40].
5. For elements marked for refinement in the coarse mesh \mathcal{T}_H determine whether to perform h - or p -refinement; see, for example, [26, 31, 32, 40].
6. Perform mesh smoothing of the fine mesh to ensure that for any coarse element $K \in \mathcal{T}_h$ marked for h -refinement that $\mathcal{T}_h(K)$ contains at least 2^d fine mesh elements. Also, for any coarse mesh element $K \in \mathcal{T}_H$ marked for p -refinement, if there exists a fine mesh element $\kappa \in \mathcal{T}_h(K)$ such that $p_\kappa = P_K$ do not perform p -refinement on K .
7. Perform hp -refinement on the coarse mesh.

Here, $\lambda_F, \lambda_C \in (0, \infty)$ are steering parameters selected such that $\lambda_F \lambda_C \leq 1$.

Remark 4.3. For the purposes of the numerical experiments in the following section the initial coarse mesh, in Step 2 above, is selected by agglomerating the fine mesh into $\lceil N/2^d \rceil$ coarse elements, where N is the number of fine mesh elements, and the initial polynomial degrees for all fine and coarse elements are set to the same polynomial degree; i.e., for a polynomial degree p we set $p_\kappa = p$ for all $\kappa \in \mathcal{T}_h$ and $P_K = p$ for all $K \in \mathcal{T}_H$.

In order to perform refinement on the coarse element we need an algorithm for h -refinement of agglomerated elements. The first potential algorithm is a naïve approach based on simply agglomerating the sub-elements on a coarse element marked for refinement into smaller elements; cf. [16].

Algorithm 4.4 (Naïve (Unweighted) Coarse Refinement). For each $K \in \mathcal{T}_H$ marked for refinement partition the sub-patch $\mathcal{T}_h(K)$ into 2^d elements using graph partitioning (e.g., by METIS [28]).

The standard graph partitioning algorithm subdivides the elements into partitions containing a roughly equal number of elements. However, given that we have information on the likely local error size for each fine mesh element, it should be possible to refine the coarse mesh elements to equidistribute the magnitude of the error indicators to the new elements. To this end, we note that METIS provides a means of performing graph partitioning based on allocating weights for each vertex, cf. [27]. Exploiting this procedure, we propose the following alternative algorithm.

Algorithm 4.5 (Weighted Coarse Refinement). For each coarse element $K \in \mathcal{T}_H$ marked for refinement, we allocate some weight $\omega_\kappa \in \mathbb{R}$ to its fine sub-elements $\kappa \in \mathcal{T}_h(K)$ based on the error indicators; i.e, we set

$$\omega_\kappa = \eta_\kappa^2 + \xi_\kappa^2.$$

We then refine the coarse element $K \in \mathcal{T}_H$ as follows:

1. Construct an adjacency graph for $\mathcal{T}_h(K)$, with a vertex \mathcal{N}_κ for each element $\kappa \in \mathcal{T}_h(K)$, and an edge \mathcal{E}_F connecting the vertices $\mathcal{N}_\kappa, \mathcal{N}_{\kappa'}$ of each pair of elements κ, κ' which share a common face $F \in \mathcal{F}_h^\mathcal{I}(K) := \{F \in \mathcal{F}_h^\mathcal{I} : F = \partial\kappa \cap \partial\kappa', \kappa, \kappa' \in \mathcal{T}_h(K)\}$.
2. Assign the weights ω_κ to the vertex \mathcal{N}_κ for each element $\kappa \in \mathcal{T}_h(K)$.
3. Perform graph partitioning on the adjacency graph to partition the graph into 2^d sub-graphs such that the sum of the weights in each sub-graph is (roughly) equal.
4. Construct the new refined elements from the sub-graphs.

Note, this algorithm is performed after fine mesh refinement; therefore, we divide the error indicators η_κ and ξ_κ of a refined fine mesh element $\kappa \in \mathcal{T}_h$ between its new elements. To that end, we change the fine mesh refinement algorithm to compute new *effective* error indicators:

Algorithm 4.6. We calculate the *effective* error indicators η'_κ and ξ'_κ on the fine mesh after mesh refinement from η_κ and ξ_κ as follows.

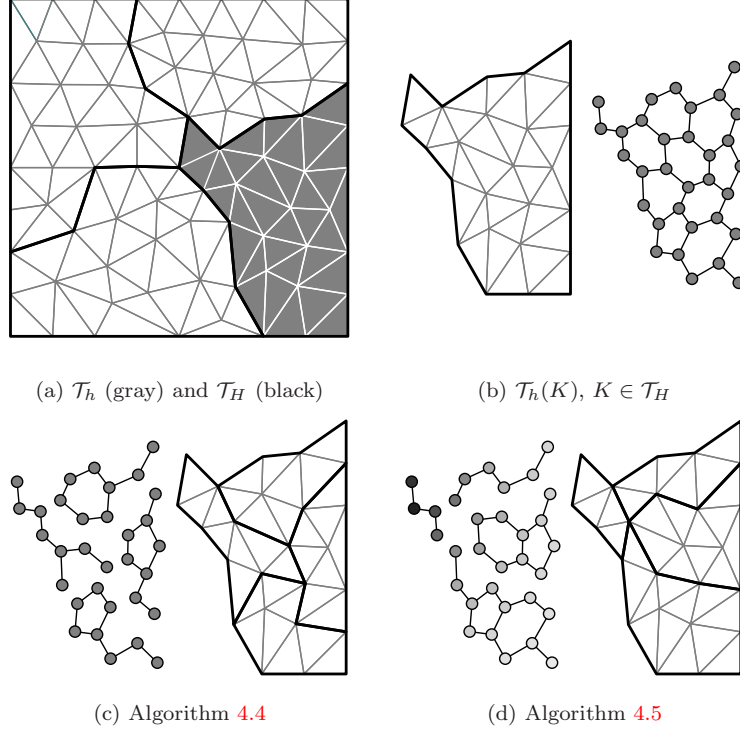


Figure 1: Coarse element refinement example. (a) Fine mesh (gray) agglomerated into 4 coarse elements (black), with shaded element $K \in \mathcal{T}_H$ marked for h -refinement; (b) The element $K \in \mathcal{T}_H$ marked for h -refinement, the constituent fine elements $\mathcal{T}_h(K)$, and the adjacency graph for these fine elements. (c) Algorithm 4.4. Graph partitioning of the adjacency graph, and the resulting coarse element refinement. (d) Algorithm 4.5. Graph partitioning of the adjacency graph with vertex weights $\omega_\kappa = \eta_\kappa^2 + \xi_\kappa^2$, $\kappa \in \mathcal{T}_h(K)$, denoted by vertex color (black = 0.5, white = 0), and the resulting coarse element refinement

```

for all  $\kappa \in \mathcal{T}_h$  do
  if  $\kappa$  is marked for  $h$ -refinement then
    Perform  $h$ -refinement, dividing the element into  $N$  children:  $\kappa_1, \dots, \kappa_N$ 
     $\eta'_{\kappa_i} \leftarrow \frac{\eta_\kappa}{\sqrt{N}}$ , for  $i = 1, \dots, N$ 
     $\xi'_{\kappa_i} \leftarrow \frac{\xi_\kappa}{\sqrt{N}}$ , for  $i = 1, \dots, N$ 
  else
     $\eta'_{\kappa} \leftarrow \eta_\kappa$ 
     $\xi'_{\kappa} \leftarrow \xi_\kappa$ 
  end if
end for

```

Fig. 1 demonstrates Algorithms 4.4 & 4.5 for an example coarse element refinement. Fig. 1(a) shows an example fine mesh \mathcal{T}_h with corresponding coarse mesh \mathcal{T}_H constructed by agglomerating the fine mesh into four elements, and highlights one coarse element $K \in \mathcal{T}_H$ for h -refinement. In Fig. 1(b) we take the constituent fine elements $\mathcal{T}_h(K)$ of the element $K \in \mathcal{T}_H$ marked for h -refinement and create the matching adjacency graph for these elements. Figs. 1(c) & 1(d) show how Algorithm 4.4 and Algorithm 4.5, respectively, partition the adjacency graph into $2^d = 4$ sub-graphs, and the matching coarse element refinement.

5 Numerical experiments

In this section we perform a series of numerical experiments to demonstrate the performance of the *a posteriori* error bound stated in Theorem 4.1, the *hp*-adaptive mesh refinement strategy outlined in Algorithm 4.2, and the coarse mesh refinement strategies presented in Algorithms 4.4 & 4.5, using both *h*- and *hp*-adaptive mesh refinement. We set the interior penalty parameters γ_{hp} and γ_{HP} in (6) and (10), respectively, equal to 10. For the two steering parameters from Algorithm 4.2 we set $\lambda_C = 1/2$ and $\lambda_F = 1$. The nonlinear equations are solved by employing a damped Newton iteration [33, Sect. 14.4]. The solution of the resulting set of linear equations, from either the fine mesh or at each step of the iterative nonlinear solver, is computed using either the direct MUMPS solver [1], for two-dimensional problems or an ILU preconditioned GMRES algorithm [36], for the three-dimensional problems presented here. We also calculate effectivity indices by dividing the error bound stated in Theorem 4.1, with the constant C_6 set to 1, by the error computed in the DGFEM energy norm.

For comparison purposes, for each example presented below, in addition to the *h*- and *hp*-version adaptive two-grid algorithms presented in Section 4, we also perform *h*- and *hp*-adaptive refinement using the standard DGFEM formulation (5).

5.1 Example 1: Smooth analytical solution

In this example, we let Ω be the unit square $(0, 1)^2 \subset \mathbb{R}^2$, define the nonlinear coefficient by

$$\mu(|\nabla u|) = 2 + \frac{1}{1 + |\nabla u|}, \quad (17)$$

and select the forcing function f such that the analytical solution to (1) is given by

$$u(x, y) = x(1 - x)y(1 - y)(1 - 2y)e^{-20(2x-1)^2}.$$

In Fig. 2(a) we present the relative error measured in the energy norm versus the third root of the number of degrees of freedom (in the fine finite element space $V_{hp}(\mathcal{T}_h, \mathbf{p})$) for the standard DGFEM formulation (5), together with the corresponding quantities computed based on employing the two-grid DGFEM formulation (8)–(9) using both Algorithm 4.4 (TG Unweighted) and Algorithm 4.5 (TG Weighted) for the coarse mesh refinement. Here, we perform both *h*- and *hp*-adaptive refinement for all methods (independently). We observe that, for the problem at hand, when *h*-refinement is employed the two two-grid methods lead to a slight increase in the error measured in the DGFEM norm, relative to the standard DGFEM formulation, in the sense that for a fixed number of degrees of freedom the latter is slightly superior. In the *hp*-refinement setting, we note that exponential convergence is observed for all three methods as the underlying finite element space is enriched, although we notice that when unweighted coarse mesh refinement procedure, cf. Algorithm 4.4, is employed within the two-grid method, then the norm of the error has a noticeably slower rate of convergence. In Fig. 2(b), we display the effectivity indices calculated by dividing the error bound by the true error measured in the energy norm for each of DGFEMs and refinement strategies employed. We note that initially the effectivity indices drop before roughly stabilizing to a constant, thus indicating that the *a posteriori* error bound overestimates the true error by a roughly consistent amount.

Although Fig. 2(a) suggests that the two-grid methods perform worse than the standard DGFEM, when considering the magnitude of the error measured in the DGFEM norm relative to the number of degrees of freedom employed in the fine finite element space $V_{hp}(\mathcal{T}_h, \mathbf{p})$, this degradation is expected since we are only solving a linearized version of the underlying numerical scheme on $V_{hp}(\mathcal{T}_h, \mathbf{p})$. However, as the coarse space $V_{HP}(\mathcal{T}_H, \mathbf{P})$ should contain considerably fewer degrees of freedom than $V_{hp}(\mathcal{T}_h, \mathbf{p})$, we expect the two-grid method to be computationally cheaper as it only solves the nonlinear problem on $V_{HP}(\mathcal{T}_H, \mathbf{P})$. With this mind, in Fig. 2(c) we compare the number of degrees of freedom in $V_{HP}(\mathcal{T}_H, \mathbf{P})$ and $V_{hp}(\mathcal{T}_h, \mathbf{p})$ for both coarse mesh refinement strategies, Algorithms 4.4 & 4.5, when both *h*- and *hp*-refinement are employed. As expected, the

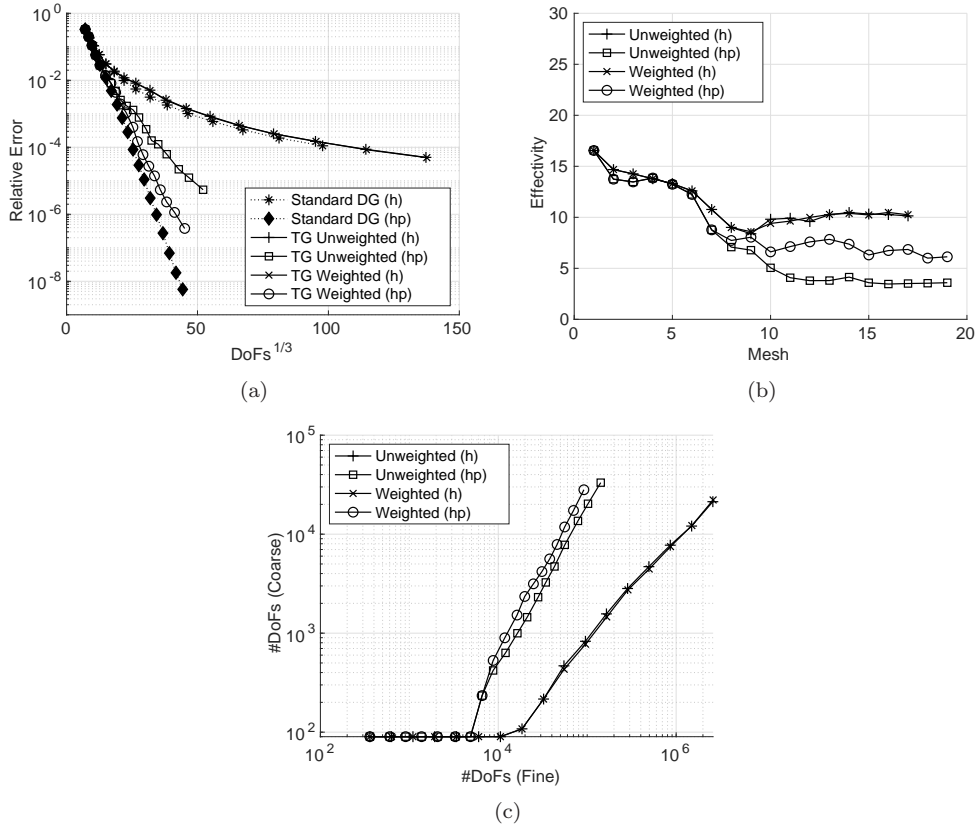


Figure 2: Example 1. (a) Error in the DG norm with respect to the number of degrees of freedom for the standard method and the two-grid methods, using weighted and unweighted coarse mesh refinement, with h - and hp -refinement; (b) Effectivity indices for the two-grid method with h - and hp -refinement; (c) Comparison of the number of degrees of freedom on the coarse and fine mesh for the two-grid methods

number of degrees of freedom in the coarse mesh is considerably lower compared to the fine mesh; furthermore, we notice that both the unweighted, Algorithm 4.4, and weighted, Algorithm 4.5, coarse mesh refinement algorithms result in a similar number of coarse mesh degrees of freedom compared to the fine mesh.

To investigate this issue further in Fig. 3, we compare the relative error computed in the energy norm with the cumulative computation time for both the standard DGFEM and the two two-grid DGFEMs employing the different coarse mesh refinement strategies, when both h - and hp -adaptive mesh refinement is exploited. In the h -refinement setting the two two-grid DGFEMs lead to around an order of magnitude decrease in the error measured in the DGFEM norm, when compared to the standard DGFEM, for a given fixed computation time. When hp -refinement is employed, the reduction in the error in the two-grid DGFEM compared to the standard DGFEM, for a given fixed amount of computation time, increases to roughly two orders of magnitude when the weighted coarse mesh refinement strategy, cf. Algorithm 4.5, is employed. However, when the unweighted coarse mesh refinement algorithm is employed within the two-grid DGFEM, cf. Algorithm 4.4, this improvement in the error computed in the DGFEM norm decreases as refinement progresses; this is caused by the noticeably slower rate of convergence observed in Fig. 2(a). This result, along with the fact that both coarse mesh refinement algorithms result in a broadly similar number of degrees of freedom on the coarse mesh, suggest that the weighted Algorithm 4.5 coarse mesh refinement is a superior refinement strategy in the hp -setting.

Finally, in Fig. 4 we show the fine and coarse meshes after 8 h - and hp -adaptive refinements

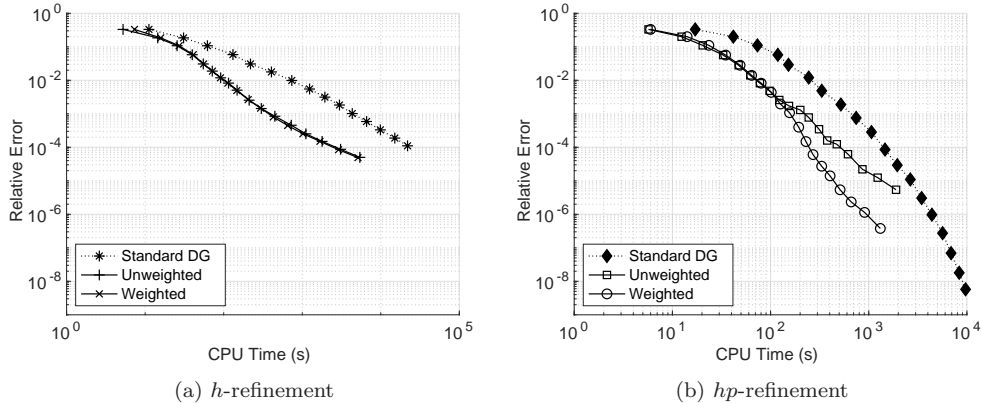


Figure 3: Example 1. Error in the DG norm with respect to the cumulative CPU time for the standard method and the two-grid methods, using weighted and unweighted coarse mesh refinement, with (a) h - and (b) hp -refinement

for the two-grid method using the weighted, cf. Algorithm 4.5, coarse mesh refinement strategy, where the shading indicates the polynomial degree for the hp -refinement case. We notice that the refinement is concentrated around the ‘hills’ in the analytical solution for both meshes, with mostly p -refinement in the interior, as would be expect when employing the standard DGFEM. We note considerably less refinement in the coarse hp -mesh compared to the fine one.

5.2 Example 2: Singular solution

In this example we consider the L-shaped domain $\Omega = (-1, 1)^2 \setminus [0, 1] \times (-1, 0] \subset \mathbb{R}^2$ and select the nonlinear coefficient to be

$$\mu(|\nabla u|) = 1 + e^{-|\nabla u|^2}.$$

By writing (r, φ) to denote the system of polar coordinates, we choose the forcing function f and impose inhomogeneous boundary conditions such that the analytical solution to (1) is given by

$$u(r, \varphi) = r^{2/3} \sin\left(\frac{2}{3}\varphi\right).$$

Note that u is analytic in $\overline{\Omega} \setminus \{\mathbf{0}\}$, but ∇u is singular at the origin.

In Fig. 5(a) we again present the comparison of the relative error measured in the DGFEM energy norm versus the third root of the number of degrees of freedom in the fine space $V_{hp}(\mathcal{T}_h, \mathbf{p})$ for the standard formulation (5) and the two-grid formulation (8)–(9) using both coarse mesh refinement strategies, Algorithm 4.4 and Algorithm 4.5, when h - and hp -refinement is employed. Here, we note that for hp -refinement the two two-grid methods again lead to a slight degradation in the error measured in the DGFEM norm, for a fixed number of degrees of freedom, when compared to the standard DGFEM. Additionally, we again observe that the two-grid DGFEM employing the weighted, cf. Algorithm 4.5, coarse mesh refinement strategy performs slightly better than the corresponding scheme exploiting the unweighted, cf. Algorithm 4.4, strategy. In the h -refinement setting, we actually observe the opposite behaviour: namely, that the two two-grid methods lead to a reduction in the error computed in the DGFEM norm, for a fixed number of degrees of freedom, when compared to the standard DGFEM, which is quite unexpected. Fig. 5(b) again shows the effectivity indices for both two-grid refinement strategies using h - and hp -refinement; here, we observe that they are almost constant for all meshes indicating that the *a posteriori* error bound overestimates the true error in a roughly consistent manner. Fig. 5(c) again shows the coarse space degrees of freedom increasing at a slower rate compared to the corresponding quantity for the fine space for both two-grid DGFEMs employing either h - or hp -mesh refinement strategies; indeed,

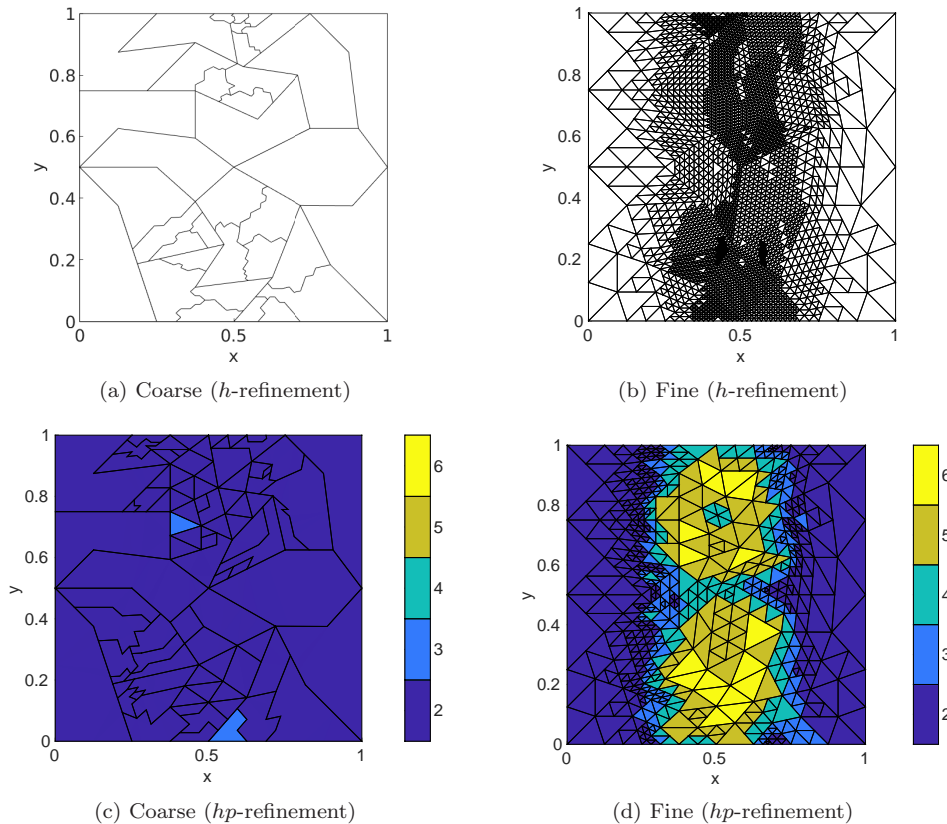


Figure 4: Example 1. Coarse and fine meshes after 8 (a)–(b) h - and (c)–(d) hp -adaptive mesh refinements, respectively

both methods result in a broadly similar number of coarse space degrees of freedom, although with slightly more coarse space degrees of freedom in the weighted hp -refinement case.

In Fig. 6 we again compare the relative error computed in the DGFEM energy norm against the cumulative computation time for the standard DGFEM and both two-grid methods utilizing weighted and unweighted refinement of the coarse space. While we again notice a reduction in the DGFEM norm of error, for a given fixed computation time, when the two two-grid methods are employed compared to the standard DGFEM, this reduction is smaller than observed for the first example.

In Fig. 7 we show the coarse and fine meshes after 8 h - and hp -adaptive mesh refinements for the two-grid method using the weighted Algorithm 4.5 coarse mesh refinement strategy. Here, we notice that for both coarse and fine meshes that the h -refinement is concentrated around the singularity at the re-entrant corner, with bands of p -refinement around this. We notice considerably more refinement on the coarse mesh compared with the previous example, caused by the method needing to resolve the singularity on both meshes.

5.3 Example 3: 3D singular solution

Finally, we consider a three-dimensional problem; to this end, we let Ω be the Fichera corner $(-1, 1)^3 \setminus [0, 1)^3 \subset \mathbb{R}^3$, use the nonlinearity (17) from the first example and select f and a suitable inhomogeneous boundary condition such that the analytical solution to (1) is given by

$$u(x, y, z) = (x^2 + y^2 + z^2)^{q/2},$$

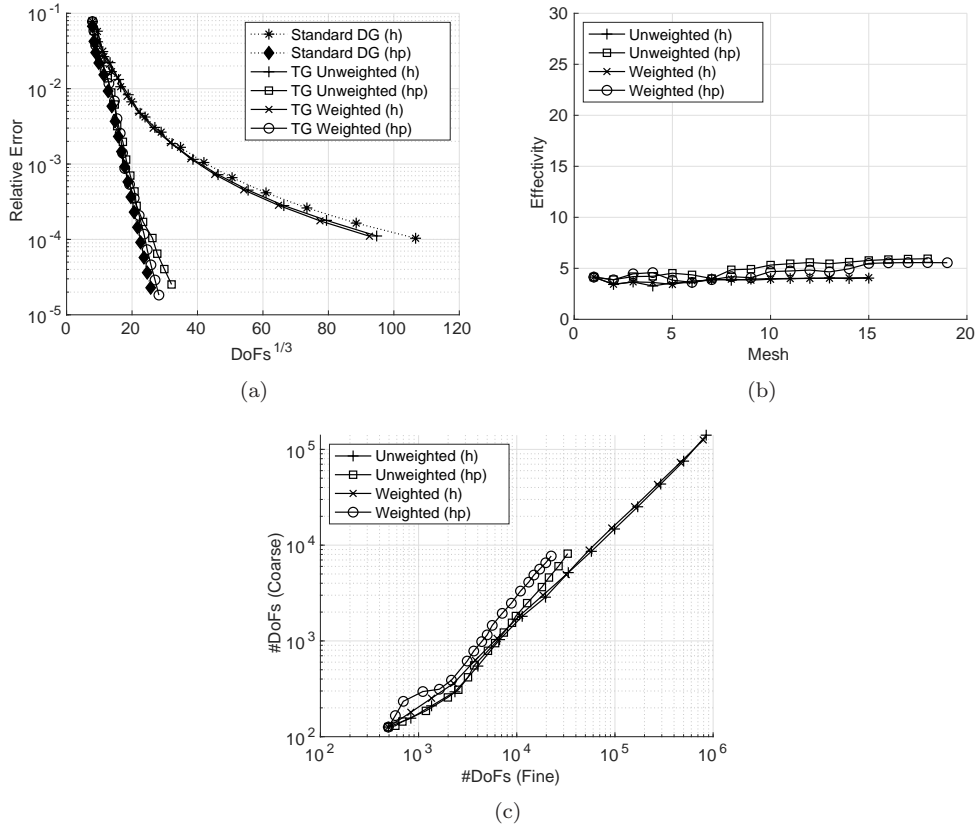


Figure 5: Example 2. (a) Error in the DG norm with respect to the number of degrees of freedom for the standard method and the two-grid methods, using weighted and unweighted coarse mesh refinement, with h - and hp -refinement; (b) Effectivity indices for the two-grid method with h - and hp -refinement; (c) Comparison of the number of degrees of freedom on the coarse and fine mesh for the two-grid methods

where $q \in \mathbb{R}$. From [9] we note that for $q \geq -1/2$ the solution satisfies $u \in H^1(\Omega)$; in this case we select $q = -1/4$ as in [46]. We note that this gives a singularity at the re-entrant corner.

In Fig. 8(a) we compare the relative error measured in the DGFEM norm with the fourth root, cf. [46], of the number of degrees of freedom in $V_{hp}(\mathcal{T}_h, \mathbf{p})$ for each of three methods considered in the previous examples, when h - or hp -refinement is employed. We again notice that for hp -refinement we obtain exponential convergence, with a slightly slower rate when the two-grid methods are employed compared to the standard DGFEM; in the h -refinement setting the two two-grid methods lead to a reduction in the computed error, for a fixed number of degrees of freedom, when compared the standard DGFEM. Fig. 8(b) confirms that the *a posteriori* error estimate again overestimates the error by a consistent amount in the sense that the effectivity indices for the two-grid methods employing both coarse mesh refinement strategies are roughly constant. Again, we observe that the coarse number of degrees of freedom grows slower than the number of degrees of freedom present in fine space, with a broadly similar number of degrees of freedom for both coarse mesh refinement strategies, cf. Fig. 8(c).

We finally compare the relative error measured in the energy norm against the cumulative computation time taken for the standard DGFEM and the two two-grid methods employing both coarse mesh refinement strategies, for h - and hp -refinement; cf. Fig. 9. As for the previous example we notice a small reduction in the error for a fixed computation time when the two grid methods are employed compared with the standard DGFEM.

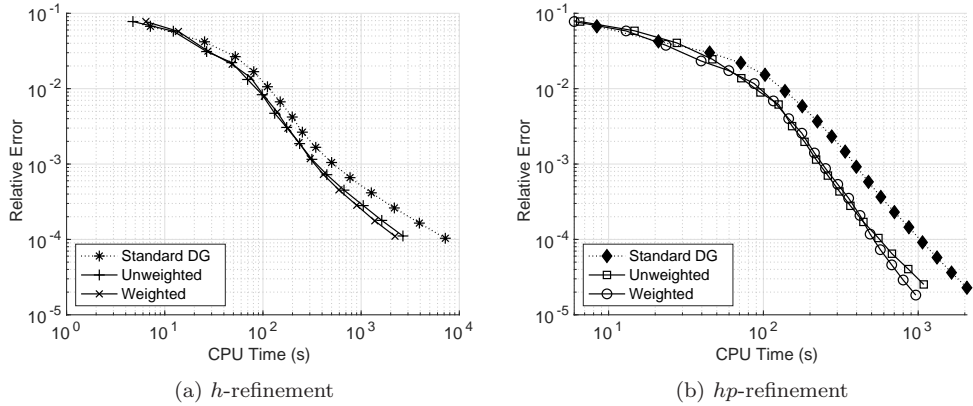


Figure 6: Example 2. Error in the DG norm with respect to the cumulative CPU time for the standard method and the two-grid methods, using weighted and unweighted coarse mesh refinement, with (a) h - and (b) hp -refinement

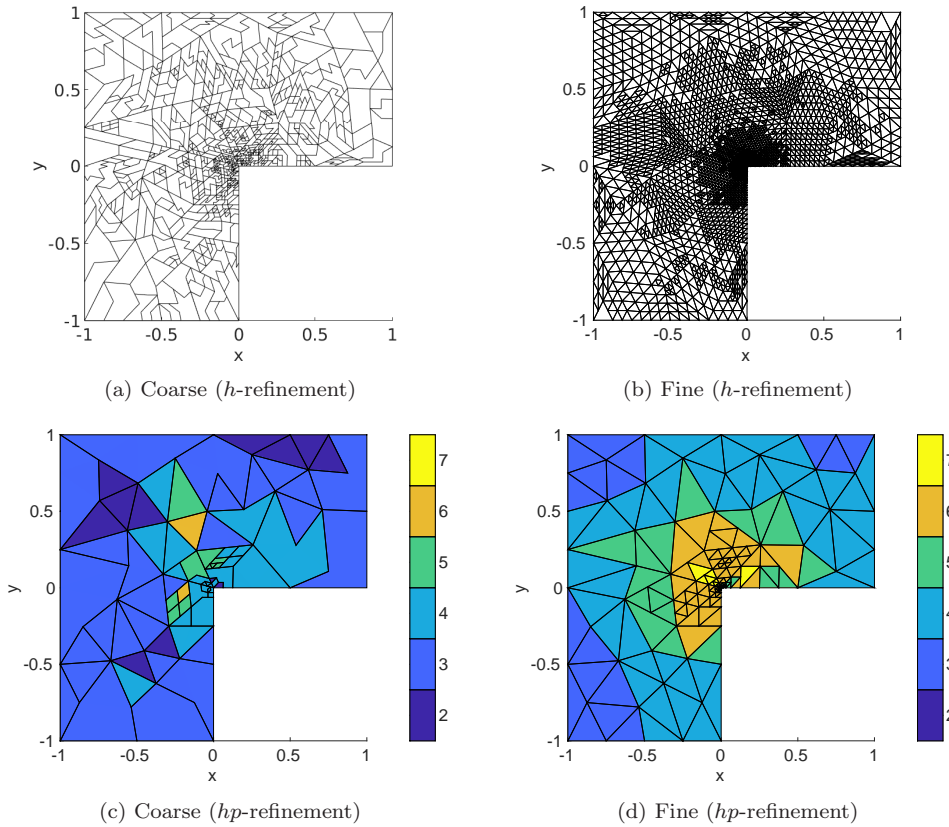


Figure 7: Example 2. Coarse and fine meshes after 8 (a)–(b) h - and (c)–(d) hp -adaptive mesh refinements, respectively

6 Concluding remarks

In this article, we have extended previous work on two-grid hp -version DGFEMs for the numerical approximation of second-order quasilinear boundary value problems of monotone type to the situation when general coarse meshes containing polytopic elements constructed by the agglomeration

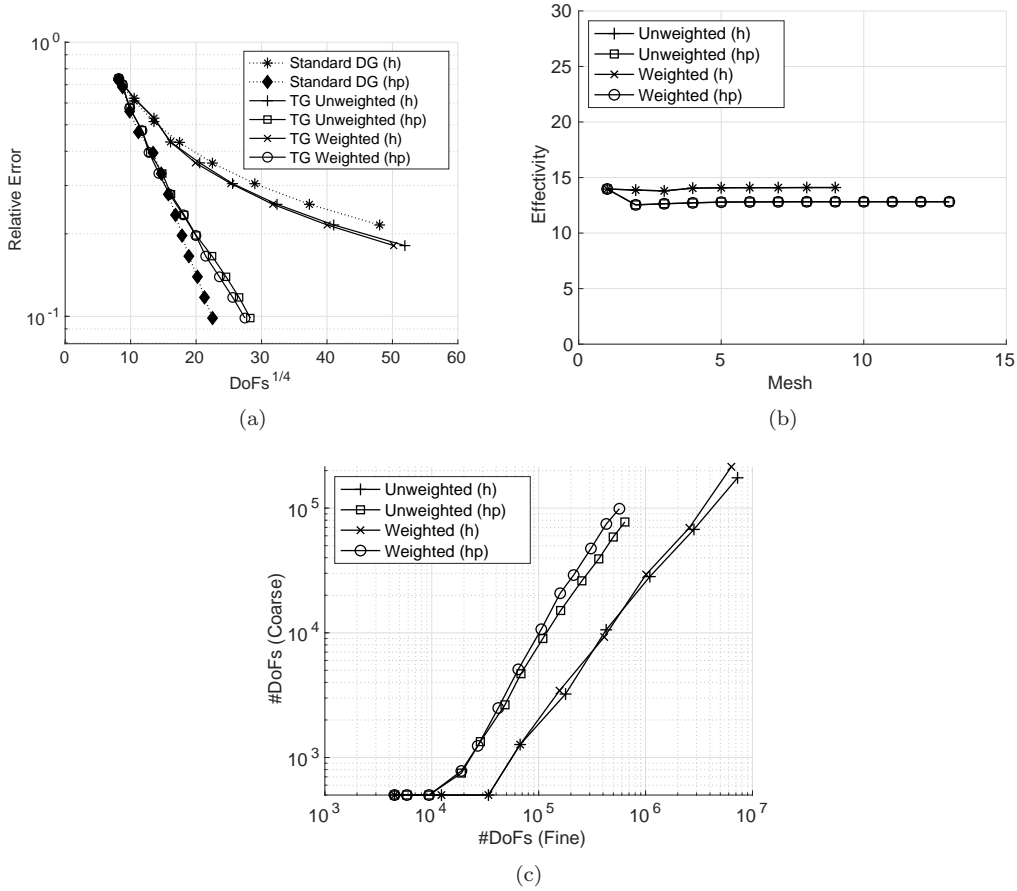


Figure 8: Example 3. (a) Error in the DG norm with respect to the number of degrees of freedom for the standard method and the two-grid methods, using weighted and unweighted coarse mesh refinement, with h - and hp -refinement; (b) Effectivity indices for the two-grid method with h - and hp -refinement; (c) Comparison of the number of degrees of freedom on the coarse and fine mesh for the two-grid methods

of fine mesh elements are employed. In particular, we have developed the *a priori* error analysis for the polytopic coarse mesh approximation and developed algorithms for hp -adaptive refinement of the coarse mesh elements based on a computable *a posteriori* error bound. This leads to fully adaptive black-box solver which can be used for the numerical approximation of nonlinear PDEs in an efficient manner. Indeed, our numerical experiments have highlighted that the computed error in the proposed two-grid method is generally similar in magnitude to the corresponding quantity computed based on employing a standard DGFEM formulation; however, the need to only solve a nonlinear system of equations on the coarse finite element space, with only a linear problem computed on the fine space, leads to significant reductions in the overall computation time when the former approach is employed. We have also shown that by weighting the refinement of the coarse mesh elements by the localized *a posteriori* error indicators defined on the submesh partition that forms the coarse element, we are able to reduce the error compared to both the number of degrees of freedom in the fine finite element space and the overall computation time. Further extensions of this work include the application to PDE problems with coefficients containing more general nonlinearities.

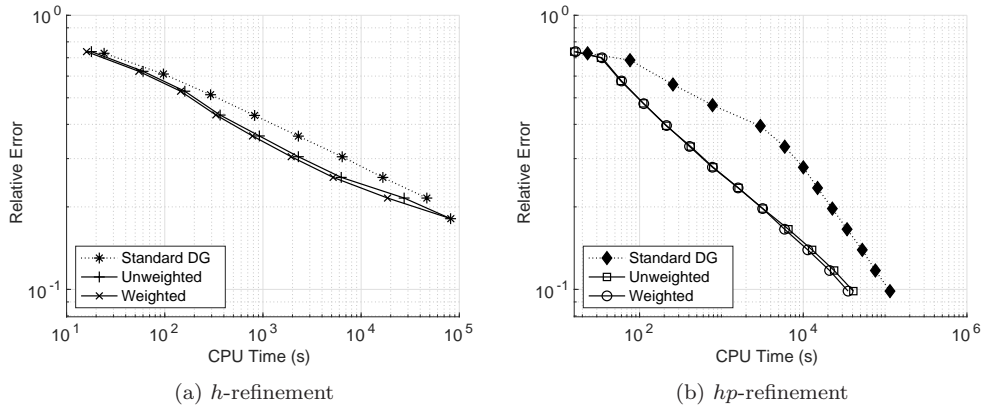


Figure 9: Example 3. Error in the DG norm with respect to the cumulative CPU time for the standard method and the two-grid methods, using weighted and unweighted coarse mesh refinement, with (a) h - and (b) hp -refinement

Acknowledgments

SC has been supported by Charles University Research program No. UNCE/SCI/023 and the Czech Science Foundation (GAČR) project No. 20-01074S. PH acknowledges the financial support of the EPSRC under the grant EP/R030707/1.

References

- [1] P. Amestoy, I. Duff, and J.-Y. L’Excellent. Multifrontal parallel distributed symmetric and unsymmetric solvers. *Comput. Methods Appl. Mech. Engrg.*, 184:501–520, 2000.
- [2] P. Antonietti, S. Giani, and P. Houston. hp -Version composite discontinuous Galerkin methods for elliptic problems on complicated domains. *SIAM J. Sci. Comput.*, 35(3):A1417–A1439, 2013.
- [3] P. F. Antonietti, C. Facciola, P. Houston, I. Mazzieri, G. Pennesi, and M. Verani. High-order discontinuous galerkin methods on polyhedral grids for geophysical applications: Seismic wave propagation and fractured reservoir simulations. In D. A. Di Pietro, L. Formaggia, and R. Masson, editors, *Polyhedral Methods in Geosciences*, pages 159–225. Springer International Publishing, Cham, 2021.
- [4] P. F. Antonietti, P. Houston, X. Hu, M. Sarti, and M. Verani. Multigrid algorithms for hp -version interior penalty discontinuous Galerkin methods on polygonal and polyhedral meshes. *Calcolo*, 54(4):1169–1198, 2017.
- [5] P. F. Antonietti, P. Houston, G. Pennesi, and E. Süli. An agglomeration-based massively parallel non-overlapping additive Schwarz preconditioner for high-order discontinuous galerkin methods on polytopic grids. *Math. Comp.*, 89:2047–2083, 2020.
- [6] P. F. Antonietti and G. Pennesi. V -cycle multigrid algorithms for discontinuous Galerkin methods on non-nested polytopic meshes. *J. Sci. Comput.*, 78(1):625–652, 2019.
- [7] O. Axelsson and W. Layton. A two-level method for the discretization of nonlinear boundary value problems. *SIAM J. Numer. Anal.*, 33(6):2359–2374, 1996.
- [8] F. Bassi, L. Botti, and A. Colombo. Agglomeration-based physical frame dG discretizations: An attempt to be mesh free. *Math. Model. Methods Appl. Sci.*, 24(8):1495–1539, 2014.

- [9] L. Beilina, S. Korotov, and M. Křížek. Nonobtuse tetrahedral partitions that refine locally towards Fichera-like corners. *App. Math.*, 50(6):569–581, 2005.
- [10] L. Beirão da Veiga, K. Lipnikov, and G. Manzini. *The mimetic finite difference method for elliptic problems*, volume 11 of *MS&A. Modeling, Simulation and Applications*. Springer, Cham, Switzerland, 2014.
- [11] C. Bi and V. Ginting. Two-grid finite volume element method for linear and nonlinear elliptic problems. *Numer. Math.*, 108:177–198, 2007.
- [12] C. Bi and V. Ginting. Two-grid discontinuous Galerkin method for quasi-linear elliptic problems. *J. Sci. Comput.*, 49:311–331, 2011.
- [13] A. Cangiani, Z. Dong, E. H. Georgoulis, and P. Houston. *hp-version Discontinuous Galerkin Methods of Polygonal and Polyhedral Meshes*. Springer Briefs in Mathematics. Springer, Cham, Switzerland, 2017.
- [14] A. Cangiani, E. Georgoulis, and P. Houston. *hp-Version discontinuous Galerkin methods on polygonal and polyhedral meshes*. *Math. Model. Methods Appl. Sci.*, 24(10):2009–2041, 2014.
- [15] A. Cangiani, G. Manzini, and O. J. Sutton. Conforming and nonconforming virtual element methods for elliptic problems. *IMA J. Numer. Anal.*, 37(3):1317–1354, 2017.
- [16] J. Collis and P. Houston. Adaptive discontinuous Galerkin methods on polytopic meshes. In G. Ventura and E. Benvenuti, editors, *Advances in Discretization Methods: Discontinuities, Virtual Elements, Fictitious Domain Methods*, pages 187–206. Springer International Publishing, Cham, 2016.
- [17] S. Congreve. *Two-Grid hp-Version Discontinuous Galerkin Finite Element Methods for Quasilinear PDEs*. PhD thesis, University of Nottingham, 2014.
- [18] S. Congreve and P. Houston. Two-grid *hp*-version discontinuous Galerkin finite element methods for quasi-Newtonian flows. *Int. J. Numer. Anal. Model.*, 11(3):496–524, 2014.
- [19] S. Congreve and P. Houston. Two-grid *hp*-DGFEMs on agglomerated coarse meshes. *Proc. Appl. Math. Mech.*, 19:e201900175, 2019.
- [20] S. Congreve, P. Houston, and T. P. Wihler. Two-grid *hp*-version discontinuous Galerkin finite element methods for second-order quasilinear elliptic PDEs. *J. Sci. Comput.*, 55(2):471–497, 2013.
- [21] C. N. Dawson, M. F. Wheeler, and C. S. Woodward. A two-grid finite difference scheme for non-linear parabolic equations. *SIAM J. Numer. Anal.*, 35:435–452, 1998.
- [22] D. Di Pietro and A. Ern. A hybrid high-order locking-free method for linear elasticity on general meshes. *Comput. Methods Appl. Mech. Engrg.*, 283:1–21, 2015.
- [23] T.-P. Fries and T. Belytschko. The extended/generalized finite element method: an overview of the method and its applications. *Int. J. Numer. Methods Engrg.*, 84(3):253–304, 2010.
- [24] W. Hackbusch and S. Sauter. Composite finite elements for the approximation of PDEs on domains with complicated micro-structures. *Numer. Math.*, 75:447–472, 1997.
- [25] P. Houston, J. Robson, and E. Süli. Discontinuous Galerkin finite element approximation of quasilinear elliptic boundary value problems I: the scalar case. *IMA J. Numer. Anal.*, 25:726–749, 2005.
- [26] P. Houston and E. Süli. A note on the design of *hp*-adaptive finite element methods for elliptic partial differential equations. *Comput. Methods Appl. Mech. Engrg.*, 194(2-5):229–243, 2005.

- [27] G. Karypis and V. Kumar. Multilevel algorithms for multi-constraint graph partitioning. In *SC '98: Proceedings of the 1998 ACM/IEEE Conference on Supercomputing*, 1998.
- [28] G. Karypis and V. Kumar. A fast and high quality multilevel scheme for partitioning irregular graphs. *SIAM J. Sci. Comput.*, 20(1):359–392, 1999.
- [29] W. Liu and J. Barrett. Quasi-norm error bounds for the finite element approximation of some degenerate quasilinear elliptic equations and variational inequalities. *RAIRO Modél. Math. Anal Numér*, 28(6):725–744, 1994.
- [30] M. Marion and J. Xu. Error estimates on a new nonlinear Galerkin method based on two-grid finite elements. *SIAM J. Numer. Anal.*, 32(4):1170–1184, 1995.
- [31] W. F. Mitchell and M. A. McClain. A comparison of *hp*-adaptive strategies for elliptic partial differential equations. Technical Report NISTIR 7824, National Institute of Standards and Technology, 2011.
- [32] W. F. Mitchell and M. A. McClain. A comparison of *hp*-adaptive strategies for elliptic partial differential equations. *ACM Trans. Math. Softw.*, 41(1):2:1–2:39, 2014.
- [33] J. Ortega and W. Rheinboldt. *Iterative Solution of Nonlinear Equations in Several Variables*. Computer Science and Applied Mathematics. Academic Press, New York, 1970.
- [34] C. Ortner and E. Süli. Discontinuous Galerkin finite element approximation of nonlinear second-order elliptic and hyperbolic systems. *SIAM J. Numer. Anal.*, 45(4):1370–1397, 2007.
- [35] I. Perugia and D. Schötzau. An *hp*-analysis of the local discontinuous Galerkin method for diffusion problems. *J. Sci. Comput.*, 17:561–571, 2002.
- [36] Y. Saad and M. Schultz. GMRES: A generalized minimal residual algorithm for solving nonsymmetric linear systems. *SIAM J. Sci. Stat. Comput.*, 7(3):856–869, 1986.
- [37] B. Stamm and T. Wihler. *hp*-optimal discontinuous Galerkin methods for linear elliptic problems. *Math. Comp.*, 79(272):2117–2133, 2010.
- [38] E. M. Stein. *Singular Integrals and Differentiability Properties of Functions*. Princeton University Press, Princeton, NJ, 1970.
- [39] T. Utnes. Two-grid finite element formulations of the incompressible Navier–Stokes equations. *Comm. Numer. Methods. Engng.*, 13(8):675–684, 1997.
- [40] T. Wihler. An *hp*-adaptive strategy based on continuous Sobolev embedding. *J. Comput. Appl. Math.*, 235:2731–2739, 2011.
- [41] T. Wihler, P. Frauenfelder, and C. Schwab. Exponential convergence of the *hp*-DGFEM for diffusion problems. *Comput. Math. Appl.*, 26:183–205, 2003.
- [42] L. Wu and M. Allen. Two-grid method for mixed finite-element solution of coupled reaction-diffusion systems. *Numer. Methods Partial Differ. Equ.*, 1999:589–604, 1999.
- [43] J. Xu. A new class of iterative methods for nonselfadjoint or indefinite problems. *SIAM J. Numer. Anal.*, 29:303–319, 1992.
- [44] J. Xu. A novel two-grid method for semilinear elliptic equations. *SIAM J. Sci. Comp.*, 15:231–237, 1994.
- [45] J. Xu. Two-grid discretization techniques for linear and nonlinear PDEs. *SIAM J. Numer. Anal.*, 33:1759–1777, 1996.
- [46] L. Zhu, S. Giani, P. Houston, and D. Schötzau. Energy norm a-posteriori error estimation for *hp*-adaptive discontinuous Galerkin methods for elliptic problems in three dimensions. *Math. Model. Methods Appl. Sci.*, 2011.